Received: 9 January 2024 | Accepted: 6 May 2024

DOI: 10.1111/1752-1688.13211

RESEARCH ARTICLE

AMERICAN WATER RESOURCES ASSOCIATION
JAWRA
Journal of the American Water Resources Association

Streamflow response to drought in a managed coast redwood catchment

Elizabeth Keppeler[1] | Joseph Wagenbrenner[2] | Salli Dymond[3] | David Dralle[4]

[1]USDA Forest Service, Pacific Southwest Research Station, Fort Bragg, California, USA

[2]USDA Forest Service, Pacific Southwest Research Station, Arcata, California, USA

[3]School of Forestry, Northern Arizona University, Flagstaff, Arizona, USA

[4]USDA Forest Service, Pacific Southwest Research Station, Sacramento, California, USA

Correspondence
Elizabeth Keppeler, USDA Forest Service, Pacific Southwest Research Station, Fort Bragg, CA, USA.
Email: elizabeth.keppeler@usda.gov

Funding information
California Department of Forestry and Fire Protection; USDA Forest Service Pacific Southwest Research Station

Abstract

A 60-year precipitation and streamflow record from the Caspar Creek Experimental Watersheds in northern California was used to explore the propagation of meteorological drought to hydrological drought. Standardized precipitation and runoff indices were calculated for the two forested catchments using integration periods of 12, 24, and 36 months. The resulting time series were used to define three severe drought events (1976–1977, 2013–2014, and 2020–2022). The earliest drought followed the 1971–1973 harvest of the 417 ha South Fork (SF) watershed, a second followed the 1989–1992 harvest of the 479 ha North Fork watershed, and a third followed the 2017–2019 reentry harvest of the SF. From these time series, we calculated drought metrics and anomalies to model differences in catchment responses in the context of climate and management. The meteorological drought in the 1977 event was more severe and extreme than the streamflow response. Both of the 21st Century droughts were hydrologically more severe than the 1977 drought. Timber harvest initially shortened and reduced streamflow drought (1977 and 2021) but prolonged and intensified the 2014 streamflow drought. Declining fall precipitation has reduced streamflows, thereby impeding salmonid migration and exacerbating impacts on native fish. Our results provide new insights into the role of climate variation, particularly long-term and seasonal drought dynamics, in managed forests along the North American Pacific coast.

KEYWORDS
drought, streamflow, forests, watershed management

1 | INTRODUCTION

Extended droughts, which typically last longer than 6 months, produce a multitude of impacts to socio-economic and ecological systems (Heim, 2002), and present significant challenges to forest and watershed management. In the western United States, regions such as California are experiencing aridification due to warming air temperatures even without changes in annual precipitation (Williams et al., 2019). By mid-century, the spatial extent of United States (U.S.) forests subjected to severe or extreme drought is forecast to triple from an average of

Paper No. JAWR-24-0009-P of the *Journal of the American Water Resources Association* (JAWR).

Discussions are open until six months from publication.

Research Impact Statement

In coast redwood forests, streamflow deficits accruing during 21st Century droughts are taking longer to recover posing risk to fish. Forest harvest can lessen, but not eliminate streamflow drought.

11% (1991–2020) to 38% (2041–2070) of forests (Costanza et al., 2023). Projections of intensifying wet–dry annual extremes and shifts in precipitation seasonality (Swain et al., 2018; Zhang et al., 2021), along with hotter temperatures, threaten forests across much of California with drought stress (Diffenbaugh et al., 2015; Keeley & Syphard, 2021; McDowell et al., 2020; Shive et al., 2022). Trees weakened or killed by recent droughts have succumbed to beetle infestation and wildfire (Stephens et al., 2018; Vose et al., 2016), and critically low streamflows have impacted the quantity and quality of domestic water supplies (Mishra et al., 2021) as well as stream habitat for fish and other aquatic organisms (Deitch et al., 2018). Vose et al. (2016) predict that, if drought frequency and duration increase, changes in vegetation and species composition will ensue, with long-term implications for streamflow regimes, water quality, and aquatic habitat.

In forested watersheds, interactions among climate, land use, and geomorphic characteristics influence myriad ecohydrologic processes, leading to a complex range of possible outcomes. Some have suggested drought effects can be mitigated by harvesting trees (McLaughlin et al., 2013), while others suggest post-harvest regrowth may lower streamflow relative to the unharvested conditions (Ford et al., 2011). Others propose that forest resilience to drought exists where lithology limits water storage capacity in deeper underlying layers of saprolite and weathered bedrock, and seasonal precipitation exceeds the storage deficit (Dralle et al., 2018; Hahm, Dralle, et al., 2019). This storage capacity limitation allows for wet season recharge and streamflow and dry season water availability even in drought (Dralle et al., 2018; Hahm, Dralle, et al., 2019). Disentangling the impacts of drought from forest management on streamflow is difficult, in part, due to the long-term datasets that are required for such analyses. By incorporating climate data into streamflow analyses from long-term paired watershed studies, new insights into the complex hydrologic responses to forest management under differing climatic conditions can be discerned. Long-term data from paired watersheds are useful for distinguishing anthropogenic effects from the stochastic cycles of precipitation deficit and surplus (Bosch & Hewlett, 1982; Coble et al., 2020; Neary, 2016; Richardson et al., 2021a, 2023). For example, Asarian and Walker (2016) investigated trends in streamflow and precipitation in northwest California and southwest Oregon and documented a decline in September precipitation along with a decreasing trend in precipitation-adjusted streamflow due to human withdrawals and vegetation changes.

In north coastal California, two iconic tree species are vulnerable to drought. First, the coast redwood (*Sequoia sempervirens* (D. Don) Endl.) is poorly adapted to drought because it cannot easily reduce transpiration in response to declining soil moisture levels (Ambrose et al., 2015). Habitat suitability for this species is related to topographic gradients that govern soil water availability and fog frequency (Francis et al., 2020). Using dendrochronology, researchers have investigated the impacts of drought on coast redwood forest growth from central to northern California by correlating radial growth with climatic variables. Carroll et al. (2014) found that redwood radial growth declined with increasing severity of summer drought along a latitudinal gradient. Sillett et al. (2022) examined the impacts of the 2012–2015 drought on both primary (old growth) and second-growth redwoods, finding that wetter redwood sites north of 39° north latitude maintained higher productivity throughout the drought compared to drier southern sites. The second species, Douglas-fir (*Pseudotsuga mensiezii* (Mirb.) Franco), is generally considered more drought tolerant than coast redwood, and it exhibits the largest latitudinal range of commercially utilized conifers in the western United States (Hermann & Lavender, 1990). Dagley et al. (2022) studied Douglas-fir resistance, resilience, and recovery during two 21st Century drought events and reported modest declines in growth from 2007 to 2009 and larger declines during the 2012 to 2015 drought. Similarly, a large dendrochronological analysis of Douglas-fir trees across the western U.S. showed that increased temperatures can generate increases in water deficits, thereby decreasing growth in Douglas-fir trees (Restaino et al., 2016). These water deficits can even occur in the absence of meteorological drought.

Another drought-vulnerable species in the region is the endangered coho salmon (*Oncorhynchus kisutch*). Native to the coastal rivers of western North America, the coho is acutely dependent on adequate streamflows for accessing spawning habitat in fall, outmigration in spring, and rearing over the summer. Juvenile salmonid survival is diminished during years with low late-season flows (Grantham et al., 2010; May & Lee, 2011). Delayed or reduced fall rains limit the ability of adult coho to enter their natal streams to spawn (California Department of Fish and Game, 2004). In California, a trend toward drier Novembers suggests a 27-day delay in the onset of the rainy season between 1960 and 2019 (Luković et al., 2021) and a related delay in the arrival of fish-passage flows in response to this shift (Keppeler, 2016). This hydrologic regime shift toward later arrival of the stormflow season may indicate reduced opportunity for coho salmon to access spawning reaches—an issue potentially exacerbated by drought.

To aid in characterizing and comparing the hydrometeorological and ecological impacts of drought, several definitions and measures of drought have been developed over the last century (Heim, 2002; Mishra & Singh, 2010). Meteorological drought is the absence or reduction of precipitation for a period. A hydrological drought is a period of inadequate surface or subsurface water availability. There are several metrics of drought that range from simplistic rainfall deficiencies to more complex soil moisture and evapotranspiration assessments, and many of these metrics are targeted for specific aspects of resource planning (Heim, 2002). The Sixteenth World Meteorological Congress recommends that the Standardized Precipitation Index (SPI), developed by McKee et al. (1993), be used to characterize meteorological droughts (World Meteorological Organization, 2012). The SPI is derived from long-term monthly precipitation records fitted to a gamma probability distribution and standardized with a mean of zero and a standard deviation of one. It is used to assess both short- and long-term droughts for agricultural and catchment management, and provides a standardized frame of reference across locations, periods of record, and precipitation regimes (Mishra & Singh, 2010). Because the metric is standardized, it provides a simple, scaled indication of the current condition relative to the long-term record. An evaluation of drought indices for hydrologic applications found the SPI tended to capture the occurrence of streamflow droughts better than the Palmer indices (Vicente-Serrano et al., 2012).

The Standardized Runoff Index (SRI) is similar to the SPI except it is calculated using monthly streamflow rather than precipitation and is used to examine hydrological extremes, including drought (Shukla & Wood, 2008). Given the delay between precipitation and streamflow, the SRI can often better capture drought dynamics in a region as they propagate from precipitation to streams (Shukla & Wood, 2008). Saksa et al. (2017) used a 12-month SPI and SRI over a 35-year period to evaluate vegetation and evapotranspiration in three forested California catchments—Caspar Creek in the Northern Coast Ranges and Providence and Bull Creeks in the Southern Sierra Nevada—demonstrating that both the SPI and SRI successfully captured the extreme drought signal of 2014–2015. Drought indices can be used to characterize numerous metrics of interest for both meteorological and hydrological events, such as drought duration and severity, as well as the intensity of water deficits (Yevjevich, 1967).

Our objectives were to (1) compare the magnitude and timing of meteorological drought with that of streamflow drought in two rain-dominated forested catchments of California's northern coast, (2) disentangle the effects of timber harvest and climatic variation on streamflow responses to drought, (3) identify trends in precipitation amounts and seasonal distribution that may influence hydrologic response during drought, and (4) assess the effects of prior year drought on the generation of early-season flows needed for successful salmonid migration. We used the 60-year record of precipitation and streamflow in the Caspar Creek Experimental Watersheds and calculated SPI, SRI, and accumulated monthly rainfall and runoff anomalies to explore the propagation of meteorological drought (MET) to hydrological drought and subsequent recovery.

2 | METHODS

2.1 | Site description

The Caspar Creek Experimental Watersheds, established in 1961, are located within 10 km of the Pacific Ocean on the Jackson Demonstration State Forest in northern California (39.36° N, 123.74° W) (Figure 1). Due to this coastal proximity, the climate is classified as Mediterranean with cool summers (Köppen Csbn), where summer mean temperatures rarely exceed 20°C and winter minima average 5°C. Rainfall occurs mainly from October through April, with a 60-year (1963–2022) annual mean of 1146 mm. Snow is rare. Potential evapotranspiration (PET; PRISM Climate Group, 2020) exceeds mean monthly rainfall during the months of May to September. Annual runoff ratios for water years (WYs) 1963–2022 averaged 47% of total precipitation, with 95% of streamflow occurring from November to April. Fog is frequent during summer months, reducing ET and providing a small amount of precipitation input via fog drip (Keppeler, 2007; Petreshen, 2021). Soils in the area are deep loams and clay-loams (*Typic Haplohumults*) derived from uplifted marine terraces of highly fractured Pleistocene sandstone and shale. Elevations range from 40 to 330 m, with hillslopes as steep as 60°. This setting supports a highly productive coast redwood (*Sequoia sempervirens*) and Douglas-fir (*Pseudotsuga menziesii*) forest. Logging of the primary forest occurred from 1860 to 1904. The 4.17 km^2 South Fork (SF) and 4.79 km^2 North Fork (NF) catchments now support second- and third-growth forests managed for research and timber production. Detailed watershed descriptions can be found in Richardson et al. (2021a) and Dymond, Richardson, et al. (2021).

Experimental harvests removed 5% of the SF timber volume in 1967 for riparian road construction, and an additional 62% of the volume was removed during selection harvest from 1971 to 1973 (Figure 1). The NF served as the untreated experimental reference catchment until 1985, when one subcatchment (13% of watershed area) was clear-cut. Between 1989 and 1992, an additional 37% of the NF catchment was clear-cut in subcatchment units, excluding riparian areas, while four subcatchments (20%) were reserved as long-term controls (Figure 1). Subsequently, regrowth in NF clear-cuts was pre-commercially thinned by a total of about 75% in 1995, 1998, and 2001. Third-cycle logging of the SF occurred between 2017 and 2019, removing 32% of pre-harvest basal area (Dymond, Richardson, et al., 2021) (Figure 1).

2.2 | Data and analysis

Precipitation was measured using a weighing (1962–1987) or tipping bucket (1987–2022) rain gauge near the SF confluence with mainstem Caspar Creek. Gaps in daily rainfall records were reconstructed using data from a nearby gauge (within the Caspar Creek watershed) or

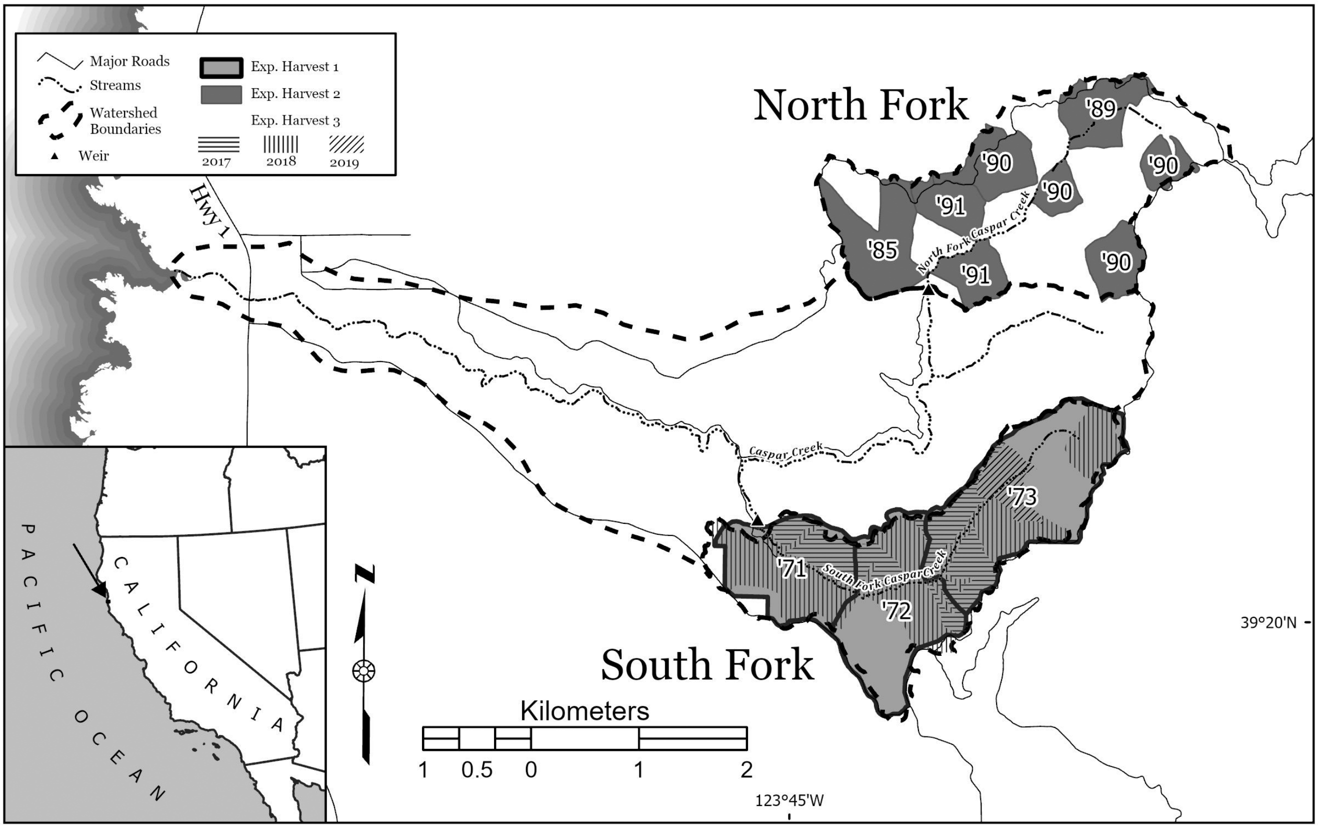

FIGURE 1 The location and experimental timber harvest history of the Caspar Creek Experimental Watersheds. Shaded areas represent logging units and are identified by a two-digit harvest year. The South Fork (SF) underwent two different experimental harvests: 1971–1973 harvest areas are indicated by shading and bounded by thick lines, and 2017–2019 harvest areas are indicated by hatching. Inset shows location in northern California.

Fort Bragg (Western Regional Climate Center station 43161). Both forks have been gauged continuously since 1962 using sharp-crested compound weirs and analog or digital stage recorders. Mean monthly flows for SF and NF weirs were tallied from chart and 10-min electronic streamflow data (Richardson et al., 2021b; Richardson, Seehafer, Keppeler, Sutherland, Wagenbrenner, Bladon, et al., 2021). Streamflow records were interrupted 11 times for sediment basin clean-outs during the drier summer months (July–September) (Richardson et al., 2020), and reconstructions for these data gaps were made using linear interpolation of stage, regression of one record on the other, or regression on mean daily flows from the Noyo River 5 km to the north (USGS gaging station # 11468500). Streamflow reconstructions account for 6% of the 60-year record in segments generally confined to the low flow season and spanning less than 2 months in duration (Table S1). The resulting monthly precipitation and streamflow time series were analyzed in this investigation (Figure 2).

For WYs 1963–2022 (October 1, 1962 to September 30, 2022), monthly SPI and SRI for the NF and SF were calculated for integration periods of 12, 24, and 36 months using the downloadable program SPI_SL6.exe (National Drought Mitigation Center, 2018). Background and computational methodology are detailed in the user guide (World Meteorological Organization, 2012). We then identified episodes of severe drought where SPI was less than −1 for at least 12 months and the intensity for the same period was less than −1.5 (Table 1). We calculated drought duration as the number of consecutive months with SPI less than −1, severity as the cumulative SPI for that duration, and intensity as the mean SPI for that duration (Mishra & Singh, 2010). We defined the extreme as the minimum SPI for the duration and persistence as the length of time the SRI remained less than the SPI following the end of drought (Table 1).

Drought events were further evaluated in terms of the maximum accumulated monthly anomaly for precipitation (AMPA) and NF or SF streamflow (AMNA and AMSA, respectively), since drought initiation. These anomalies were calculated relative to monthly means during the NF pretreatment period (reference period) of 1962–1984. The long-term precipitation record from Eureka CA (160 km to the north) indicates normal precipitation during this period (Figure S1). Annual means during this reference period were 1198 mm for precipitation, 633 mm for NF streamflow, and 645 mm for SF streamflow. Since the SF had been roaded and logged during the reference period, the mean monthly SF reference streamflow was extrapolated from the regressions of SF streamflow on NF streamflow by individual month for pre-disturbance years 1962–1967. While the monthly prediction factors and statistical results for the individual months varied, a single regression for all pre-harvest monthly data indicated a highly significant regression result ($r^2 = 0.99$, df = 60, $p < 0.0001$). The anomalies represent cumulative

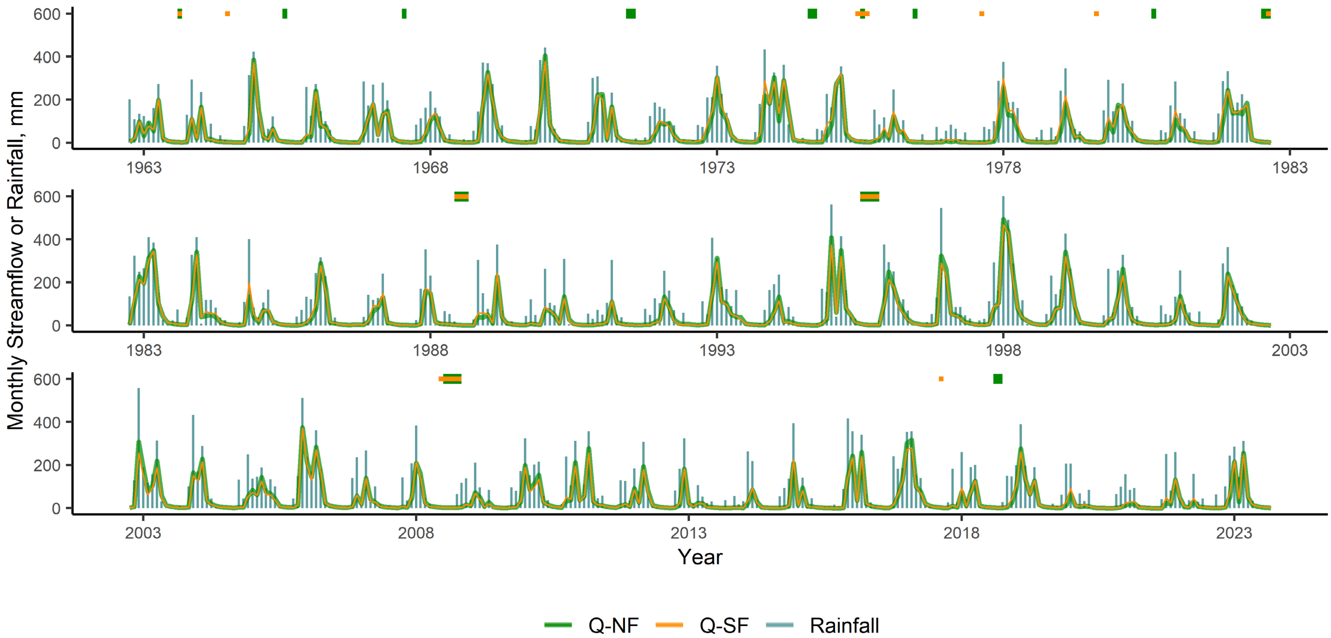

FIGURE 2 Monthly rainfall and streamflow for North Fork (Q-NF; green) and SF (Q-SF, orange) with reconstructed data gaps of more than 2 weeks indicated by line segments above the time series.

TABLE 1 Drought-related abbreviations (Abbr.) and terms used in this study.

Abbr.	Term	Explanation
SPI_n	Standardized Precipitation Index	Monthly precipitation transformed to normal distribution with a mean ($\bar{x}$) of 0 and standard deviation (s) of 1, using integration periods (*n*) of 12, 24, or 36 months: $SPI_n = \frac{x - \bar{x}}{s}$
SRI_n	Standardized Runoff Index	Monthly streamflow transformed to normal distribution with a mean of 0 and standard deviation of 1, using integration periods (*n*) of 12, 24, or 36 months
	Duration	Number of consecutive months with SPI < −1
	Severity	Cumulative SPI for duration
	Intensity	Mean SPI for duration: Intensity = Severity / Duration
	Extreme	Minimum SPI for duration
	Severe drought	Period with SPI < −1 for at least 12 consecutive months and Intensity < −1.5
	Persistence	Number of months following end of severe drought with SRI < SPI and no more than 1 month exception per period
AMPA	Accumulated monthly precipitation anomaly	Difference in precipitation relative to 1962–1984 monthly means
AMNA	Accumulated monthly NF flow anomaly	Difference in NF streamflow relative to 1962–1984 monthly means
AMSA	Accumulated monthly SF flow anomaly	Difference in SF streamflow relative to 1962–1984 monthly means
	Development	Number of consecutive months between initial reversal and climax accumulated anomaly
	Recovery	Number of consecutive months for climax accumulated anomaly to be ameliorated

absolute departures from normal conditions, here defined as the reference period precipitation and streamflow for each fork. Drought initiation was defined as the month of maximum AMPA (point of the reversal from positive to negative trend) preceding the qualifying SPI-defined drought event. Drought development was defined as the period (months) between the trend reversal in the accumulated anomaly (AMPA, AMNA, AMSA) through its maximum negative deviation and represents the period that the drought was advancing (Table 1). Recovery was the period from the month of the maximum negative anomaly to the month when the accumulated negative anomaly was ameliorated (Table 1).

We performed Mann–Kendall trend tests on monthly, seasonal, and annual precipitation and flow time series using the "Kendall" package in the R environment (McLeod, 2022; R Core Team, 2022). We also applied a generalized additive model using the "mgcv" package (R Core Team, 2022; Wood, 2011) and then assessed differences in trends between precipitation and flow using the "emtrends" function included in the "emmeans" package (Lenth et al., 2023; R Core Team, 2022). In addition, we compared precipitation and streamflow from 1985 to 2022 to the 1962–1984 reference period.

Previous research has described the effects of timber harvest on streamflow at Caspar Creek using the before-after-control-impact paired catchment regression analyses (Keppeler, 1998; Keppeler et al., 2009; Lewis, 1998; Lewis et al., 2001; Reid, 2012). Given that experimental treatments have been implemented on both NF and SF irrespective of climatic conditions, we have opted to evaluate the streamflow response to drought by comparing differences and ratios of NF and SF flow parameters and model those differences using an array of climatic and biotic variables.

We calculated the differences between the actual and mean monthly precipitation then summed these anomalies by WY to compute the annual precipitation (PPTaa) anomaly. We used the same approach to calculate the flow anomalies for the NF and SF (NFaa, SFaa). We then differenced the annual precipitation and flow anomalies for NF (Ndiff = PPTaa − NFaa) and SF (Sdiff = PPTaa − SFaa) (Table 2). We then modeled the differences between precipitation and streamflow anomalies using potentially explanatory variables defined to characterize hydrologic, climatic, and biotic parameters (Table 2) to identify the major drivers of these differences using the "leaps" package (Lumley, 2022; R Core Team, 2022). Candidate explanatory variables were screened for significant correlation with response variable ($\alpha = 0.05$) prior to model inclusion. Independent variables included temperature and PET (PRISM Climate Group, 2020), offsite radial growth indices (Carroll & Sillett, 2023), and stand inventory metrics (Continuous Forest Inventory, CFI) (California Department of Forestry and Fire Protection, unpublished data) (Table 2). CFI plot locations are within the Caspar Creek catchment area and offsite radial growth plots are within 20 km of the catchment (Figure S2). Candidate explanatory variables were standardized to facilitate comparisons of model coefficients. Model selection was based on goodness-of-fit using the Bayesian information criterion (Schwarz, 1978) to identify the most parsimonious model.

We identified the 10% exceedance flow for NF (Q_{10}) as an approximation of minimum flow for the upstream fall migration of the native coho salmon (Keppeler, 2016) on both NF and SF. We characterized the timing of this flow exceedance threshold by calculating the days between October 1 and the initial occurrence of the Q_{10} in each fork for each WY. We also summed the rainfall during each of these periods and, to reduce the additional variance introduced by precipitation well in excess of that needed to attain Q_{10}, subtracted the mean daily unit-area flow for the day the Q_{10} was achieved (NPQ_{10}adj and SPQ_{10}adj for NF and SF, respectively). We then modeled the effects of the prior year's hydrologic, meteorologic, and vegetation conditions on NPQ_{10}adj and SPQ_{10}adj. We log-transformed NPQ_{10}adj and SPQ_{10}adj in order to meet the assumption of constant variance in the residuals.

We hypothesized that prior year drought conditions might influence the magnitude of subsurface moisture deficits developing over the mostly rainless growing season, and the prior year conditions would, therefore, affect the amount of precipitation required to ameliorate this storage deficit and contribute to streamflow generation. To estimate variations in the seasonally replenished water stored in the soil and weathered substrate, we calculated dynamic catchment storage as the cumulative difference between precipitation and streamflow for fall (October to December) and winter (January to March). This assumes that ET was a relatively small component of the mass balance during the winter months, and, for the purpose of determining controls on dynamic storage, that inter-annual ET variability during the winter months was negligible. We then modeled the effect of the prior year's hydrologic conditions on these dynamic storage calculations to investigate variations related to both drought and harvest treatments. Relatedly, we calculated seasonal water balance dynamics as cumulative precipitation (PPTmm) less streamflow (NFmm, SFmm) and PET for fall (October to December), winter (January to March), spring (April to June), and summer (July to September) to assess seasonal components of drought-related variations in streamflow anomalies.

3 | RESULTS

3.1 | Drought periods

Three episodes of severe meteorological drought (MET), where the SPI was less than −1 for 12 or more months and intensity was less than −1.5, occurred within the 60-year record—1976–1977 (D1977), 2013–2014 (D2014), and 2020–2021 (D2021) (Figure 3a). D1977 was the shortest in duration but was generally more intense than D2014 and D2021 for both the 12- and 24-month integrations. D2014 was the most extreme as measured by the 12- and 24-month SPI ($SPI_{12} = -3.37$, $SPI_{24} = -2.59$). However, D2021 was the most extreme ($SPI_{36} = -2.38$) at the 36-month integration period, most severe (−45.5 and −46.1 at the 24- and 36-month integrations, respectively), and longest at the 12- and 36-month integrations, lasting 19 (SPI_{12}) to 28 (SPI_{36}) months (Table 3).

Meteorological droughts developed over 26–43 months. The accumulated monthly precipitation anomaly (AMPA) exceeded mean annual precipitation during each period of drought, and cumulative precipitation deficits were larger with each progressive drought (Table 3d). Precipitation surpluses eventually ameliorated the D1977 anomaly, achieving recovery in December 1983, but the D2014 deficit had not yet been ameliorated when D2021 began in 2019 and the D2021 had not recovered by September 2023 (Table 3d).

TABLE 2 Abbreviations for North Fork (NF) and South Fork (SF) variables. Type is hydrologic (H), climatic (C), or biotic (B). An empty SF cell means the same value was applied to NF and SF. "NA" means the term only applied to the NF.

NF	SF	Type	Definition
DR	DR	H	Proportion of days with rain = days with rain / days in period
DY12		H	Consecutive year of drought ($PPT_{12} < -0.5$)
GW_{min}	NA	H	Annual minimum groundwater depth for NF M1B1 piezometer for WY2008–2023 (m)
MClass		H	Moisture category: Dry $PPT_{12} < -1$; Normal $-1 < PPT_{12} < 1$; Wet $PPT_{12} > 1$
Ndayz	Sdayz	H	Days preceding 1st Q_{10} of WY
NdayzR	SdayzR	H	Days with PPT >0.25 mm preceding 1st Q_{10} of WY
Ndiff	Sdiff	H	Annual precipitation anomaly minus flow anomaly (mm)
NF_{12}	SF_{12}	H	SRI, September value, 12 months
NF_{24}	SF_{24}	H	SRI, September value, 24 months
NF_{36}	SF_{36}	H	SRI, September value, 36 months
NFaa	SFaa	H	Streamflow annual anomaly $= \sum_{OCT}^{SEP}(Q_{actual} - Q_{mean})$ (mm)
NFB_f	SFB_f	H	Fall water balance $= \sum_{OCT}^{DEC}(PPT - Q - PET)$ (mm)
NFB_w	SFB_w	H	Winter water balance $= \sum_{JAN}^{MAR}(PPT - Q - PET)$ (mm)
NFB_{sp}	SFB_{sp}	H	Spring water balance $= \sum_{APR}^{JUN}(PPT - Q - PET)$ (mm)
NFB_{su}	SFB_{su}	H	Summer water balance $= \sum_{JUL}^{SEP}(PPT - Q - PET)$ (mm)
NFcent	SFcent	H	Streamflow centroid, days since October 1
NFLF	SFLF	H	Low flow $= \sum_{JUL}^{SEP}(Q)$ (mm)
NFmm	SFmm	H	Streamflow (mm)
NFrr	SFrr	H	Runoff ratio = flow / precipitation
NFS_f	SFS_f	H	Fall surplus $= \sum_{OCT}^{DEC}(PPT - Q)$ (mm)
NFS_{fw}	SFS_{fw}	H	Fall + winter surplus $= \sum_{OCT}^{MAR}(PPT - Q)$ (mm)
NFS_s	SFS_s	H	Summer surplus $= \sum_{APR}^{SEP}(PPT - Q - PET)$; set to 0 if $Q + PET > PPT$ (mm)
NFS_w	SFS_w	H	Winter surplus $= \sum_{JAN}^{MAR}(PPT - Q)$ (mm)
NPQ_{10}	SPQ_{10}	H	Seasonal precipitation antecedent to 1st Q_{10} of WY (mm)
$NPQ_{10}adj$	$SPQ_{10}adj$	H	Adjusted seasonal precipitation antecedent to 1st Q_{10} of WY $= PQ_{10} - Q_{daily}$ for the day of the 1st Q_{10} (mm)
PPT_{12}		H	SPI, September value, 12 months
PPT_{24}		H	SPI, September value, 24 months
PPT_{36}		H	SPI, September value, 36 months
PPTaa		H	Precipitation annual anomaly $= \sum_{OCT}^{SEP}(Q_{actual} - Q_{mean})$ (mm)
PPT		H	Annual precipitation (mm)
Q_{10}		H	10% exceedance flow, 0.213 $m^3 s^{-1}$ [not a variable]
WY		H	Water year (Oct–Sep)
$NFET_s$	$SFET_s$	C	Summer storage deficit $= \sum_{APR}^{SEP}(PET - PPT)$ (mm)
NFMS	SFMS	C	Moisture stress $= \sum_{OCT}^{SEP}\left(1 - \frac{PPT}{PET}\right)$; monthly value = 0 if PPT > PET
NFT_{gsm}	SFT_{gsm}	C	Growing season (APR–SEP) PRISM mean monthly air temperature (°C)
NFT_{spm}	SFT_{spm}	C	Spring (APR–JUN) PRISM mean monthly air temperature (°C)
FWP_{res}		B	Fritz Wonder Plot, residual incremental growth, persistence (climate effect) removed[a]
FWP_{std}		B	Fritz Wonder Plot, standardized (detrended) incremental growth[a]
NFBAa	SFBAa	B	Basal area. NF values are pro-rated estimates from Continuous Forest Inventory (CFI)[a] and PCT plot data[b]. SF are from CFI plot data estimates ($m^2 ha^{-1}$)

TABLE 2 (Continued)

NF	SF	Type	Definition
NFHi	SFHi	B	Harvest impact within 10 years of harvest. 1st post-harvest year = 10, with stepwise decay to 0 at year 10
NR_{res}		B	Navarro Redwoods, residual incremental growth, persistence (climate effect) removed[a]
NR_{std}		B	Navarro Redwoods, standardized incremental growth (detrended)[a]
NF_SDI_{max}	SF_SDI_{max}	B	Stand Density Index,[c] derived from BA and TPA CFI plots (uncut only); divided by maximum observed for coast redwood forest (%)
TR_{res}		B	Mean of FWP_{res} and NR_{res}
TR_{std}		B	Mean of FWP_{std} and NR_{std}
UnBAa	NA	B	Basal area in uncut plots within NF, interpolated between approximate 5-year CFI measurements[c] (m^2 ha^{-1})

[a] Carroll and Sillett (2023).

[b] O'Hara et al. (2015).

[c] Jackson Demonstration State Forest (unpublished data, 2023).

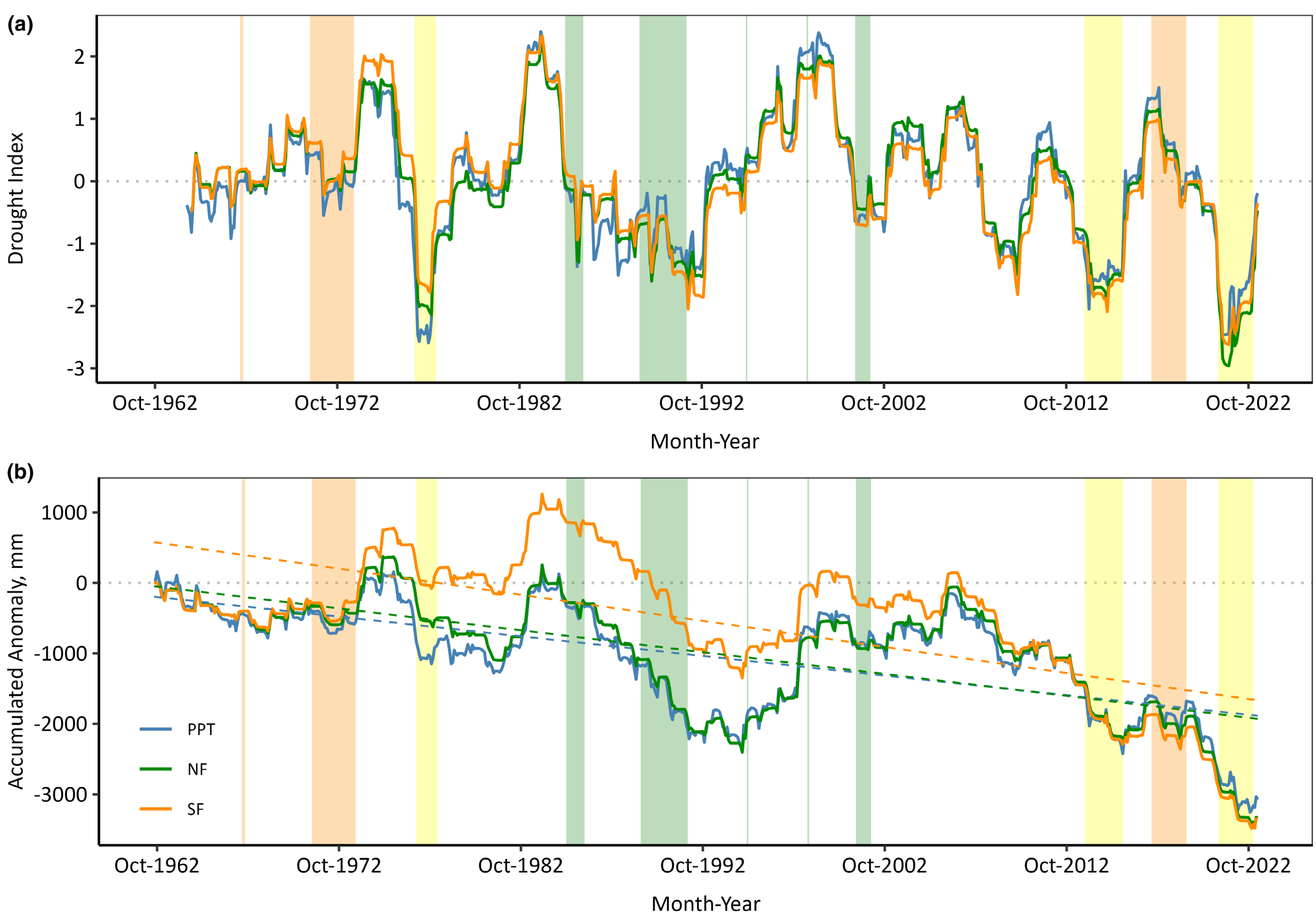

FIGURE 3 (a) Monthly drought index for precipitation (SPI_{24}) and streamflow (SRI_{24}) for NF and SF; and (b) AMPA (PPT), NF streamflow anomaly (AMNA), and SF streamflow anomaly (AMSA) relative to the 1962–1984 reference period. Trendlines for each anomaly are shown in dashed lines. Trends for AMPA and AMNA are nearly identical. Three drought periods are shaded in yellow, and harvest periods are shaded in green for the NF (50% basal area reduction by clear-cutting subcatchments in 1985–1992 and pre-commercial thinning in 1995, 1998, and 2001) and orange for the SF (road right-of-way clearing in 1967 and selection logging in 1971–1973 totaling 67% reduction; and 32% reduction by selection logging in 2017–2019).

TABLE 3 (a–c) Drought characteristics for the 1977 (D1977), 2014 (D2014), and 2021 (D2021) droughts as defined by Standardized Precipitation Index (SPI_n) and Standardized Runoff Index for NF Caspar Creek (NF_n) and SF Caspar Creek (SF_n) for different intervals: (a) 12 months ($n=12$), (b) 24 months ($n=24$), and (c) 36 months ($n=36$). (d) The accumulated monthly precipitation (AMPA) and streamflow anomalies for the NF (AMNA) and SF (AMSA) relative to the reference period (1962–1984, with means: PPT = 1198 mm, NF discharge = 633 mm, and SF discharge = 645 mm), with month and year of each maximum anomaly. Bold indicates peak metric for the interval. Characteristics are defined in Table 1.

	D1977			D2014			D2021[b]		
	October 1976–December 1977			October 2013–2014			April 2020–October 2021		
(a) 12-Months index	SPI_{12}	NF_{12}	SF_{12}	SPI_{12}	NF_{12}	SF_{12}	SPI_{12}	NF_{12}	SF_{12}
Duration, months	15	13	12	13	12	13	19	**25**	23
Severity	−36.1	−33.4	−27.1	−22.4	−22.7	−25.2	−33.9	**−49.9**	−42.5
Intensity, months^{-1}	−2.4	**−2.6**	−2.3	−1.7	−1.9	−1.9	−1.8	−2.0	−1.8
Extreme	−3.12	−3.11	−2.67	**−3.37**	−2.88	−3.19	−2.54	−3.18	−2.96
Persistence, months	NA	**19**	1	NA	6	10	NA	tbd	5
	January 1977–March 1978			October 2013–November 2015			February 2021–January 2023		
(b) 24-Months index	SPI_{24}	NF_{24}	SF_{24}	SPI_{24}	NF_{24}	SF_{24}	SPI_{24}	NF_{24}	SF_{24}
Duration, months	15	13	10	26	24	**27**	24	**27**	25
Severity	−31.3	−23.9	−16.6	−38.9	−38.2	−44.2	−45.5	**−59.3**	−52.2
Intensity, months^{-1}	−2.1	−1.8	−1.7	−1.5	−1.6	−1.6	−1.9	**−2.2**	−2.1
Extreme	−2.59	−2.14	−1.78	−2.05	−2.02	−2.09	−2.46	**−2.96**	−2.62
Persistence, months	NA	29	0	NA	**34**	**34**	NA	tbd	tbd
	February 1977–1979[a]			December 2013–February 2016			January 2021		
(c) 36-months index	SPI_{36}	NF_{36}	SF_{36}	SPI_{36}	NF_{36}	SF_{36}	SPI_{36}	NF_{36}	SF_{36}
Duration, months	25	20	0	27	27	**28**	**28**	**28**	**28**
Severity	−35.3	−23.1	NA	−41.9	−41.8	−47.24	−46.1	**−54.5**	−48.6
Intensity, months^{-1}	−1.4	−1.2	NA	−1.6	−1.5	−2	−1.6	**−1.9**	−1.7
Extreme	−1.72	−1.44	−0.73	−1.95	−2.01	−2.16	−2.38	**−2.86**	−2.6
Persistence, months	NA	**80**	0	NA	43	43	NA	tbd	tbd
(d) Anomaly	AMPA	AMNA	AMSA	AMPA	AMNA	AMSA	AMPA	AMNA	AMSA
Max. departure, mm	−1304	−995	−859	−1402	−1196	−1220	**−1579**	−1571	−1426
Max. departure, %	−109	−157	−133	−117	−189	−189	−132	**−248**	−221
Max. departure, month-year	November-1977	December-1977	November-1977	November-2015	November-2015	November-2015	November-2022	February-2023	December-2022
Development, months	26	27	26	36	36	36	43	**46**	44
Recovery, months	**73**	NA	64	NA	NA	NA	tbd	tbd	tbd

[a] D1977 as defined by 36-month index, did not meet drought definition (intensity > −1.5 and SF_{36} > −1).

[b] D2021 had not resolved as of September 2023, persistence and recovery remain to be determined (tbd).

3.2 | Streamflow responses to drought

Streamflow responses differed among the three droughts (Table 3; Figure 4). For D1977, the onset of severe streamflow drought ($SRI_{12} < -1$) lagged meteorological drought ($SPI_{12} < -1$) by 2–3 months. The recently logged (1971–1973) SF response was shorter, less severe, and less extreme than either NF or MET and exhibited almost no persistence beyond the end of the meteorological drought. In contrast, the NF SRI remained lower than the precipitation index for 19 months (12-month index) and 29 months (24-month index). D1977 streamflow deficits accrued over a period of 26 (SF) or 27 months (NF) commencing the same month as meteorological drought (November 1975). Following D1977, the SF streamflow anomaly attained positive levels 9 months earlier than precipitation (March 1983), while the NF recovery had not occurred as of the initiation of D2014 (Figure 3b).

Similar to D1977, the start of D2014 severe streamflow drought lagged meteorological drought, although only by 1–2 months (Figure 4). By the onset of D2014 (January 2013), long-term accumulated monthly anomalies were negative and similar (AMPA = −1212 mm, AMNA = −1176 mm, and AMSA = −1215 mm). Compared to D1977, the D2014 hydrological drought was longer at the 24- and 36-month integration intervals (Table 3b,c). Deficits accrued over 36 months and were larger than those of D1977. The increased duration led to greater severity and more persistent streamflow deficits on both NF and SF relative to the meteorological drought severity and deficits. The D2014 drought was more severe, intense, and extreme on SF relative to NF. The accumulated drought anomaly was also larger on SF than NF. Recovery had not occurred on either NF or SF by the time of the onset of D2021 (Table 3d; Figure 4).

D2021 was dissimilar to the prior two droughts in that hydrologically severe drought began coincident with meteorological drought, and rapidly intensified over the next 4–5 months (Figure 4). With the onset of D2021 (June 2019), streamflow indices diverged even more negatively from the SPI, resulting in greater intensity and severity and more extreme minima in the streamflow droughts as compared to meteorological drought (Table 3; Figures 4 and 5c). D2021 developed over a period of 44–46 months. When compared to reference period means, the relative accumulated runoff anomalies were larger than those of precipitation (Figure 5b) across the three droughts and increased from D1977 to D2014 and again to D2021. Streamflow anomalies for this most severe drought on record were more than twice mean annual runoff (Table 3d; Figure 5a,b).

3.3 | Trends

Mann–Kendall tests identified several significant trends in our time series (Table 4). There was no trend in annual precipitation, but precipitation declined for November ($t_{(60)} = -1.56$, $p = 0.039$), August ($t_{(60)} = -0.3$ $p = 0.001$), and fall (September to November, $t_{(60)} = -0.17$, $p = 0.027$). Fall (September to November) streamflow also declined (NF $t_{(60)} = -0.198$, $p = 0.013$ and SF $t_{(60)} = -0.287$, $p = 0.001$), though annual streamflow only declined in the SF ($t_{(59)} = -0.18$, $p = 0.021$). Relatedly, annual runoff ratios declined (NF $t_{(59)} = -0.154$, $p = 0.042$ and SF $t_{(59)} = -0.265$, $p = 0.001$) and streamflow centroids increased (NF $t_{(59)} = 0.163$, $p = 0.034$ and SF $t_{(59)} = 0.169$, $p = 0.029$) (Figure S4). A significant positive trend was detected in the number of days prior to the first Q_{10} of the WY for both forks (NF $t_{(58)} = 0.199$, $p = 0.014$ and SF $t_{(59)} = 0.222$, $p = 0.007$) and

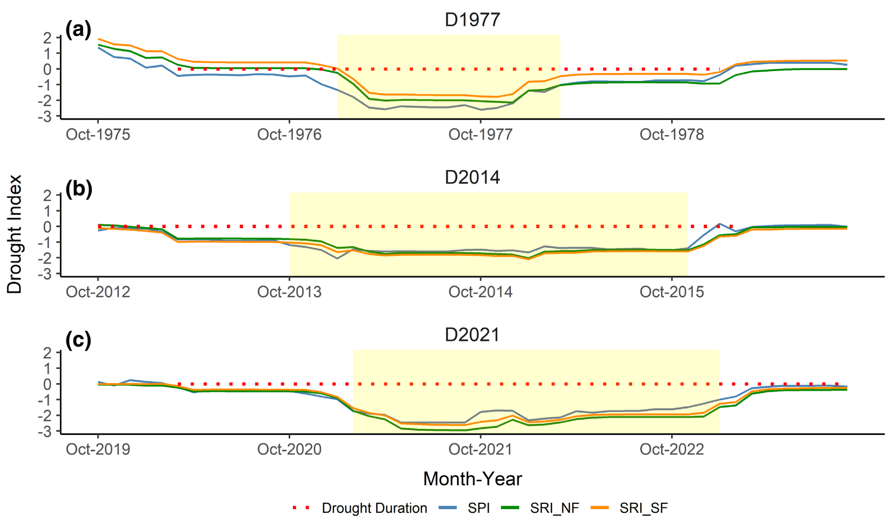

FIGURE 4 Variations in 24-month drought indices for precipitation (SPI_{24}) and runoff (NF_{24} [SRI_NF] and SF_{24} [SRI_SF]) during three severe droughts: (a) D1977, (b) D2014, and (c) D2021. Red dotted lines indicate periods of drought development (the period between initial negative SPI_{24} and maximum anomaly) and retreat (return to positive SPI_{24}). Shading (yellow) indicates the duration of a severe drought when the mean $SPI_{24} < -1.5$.

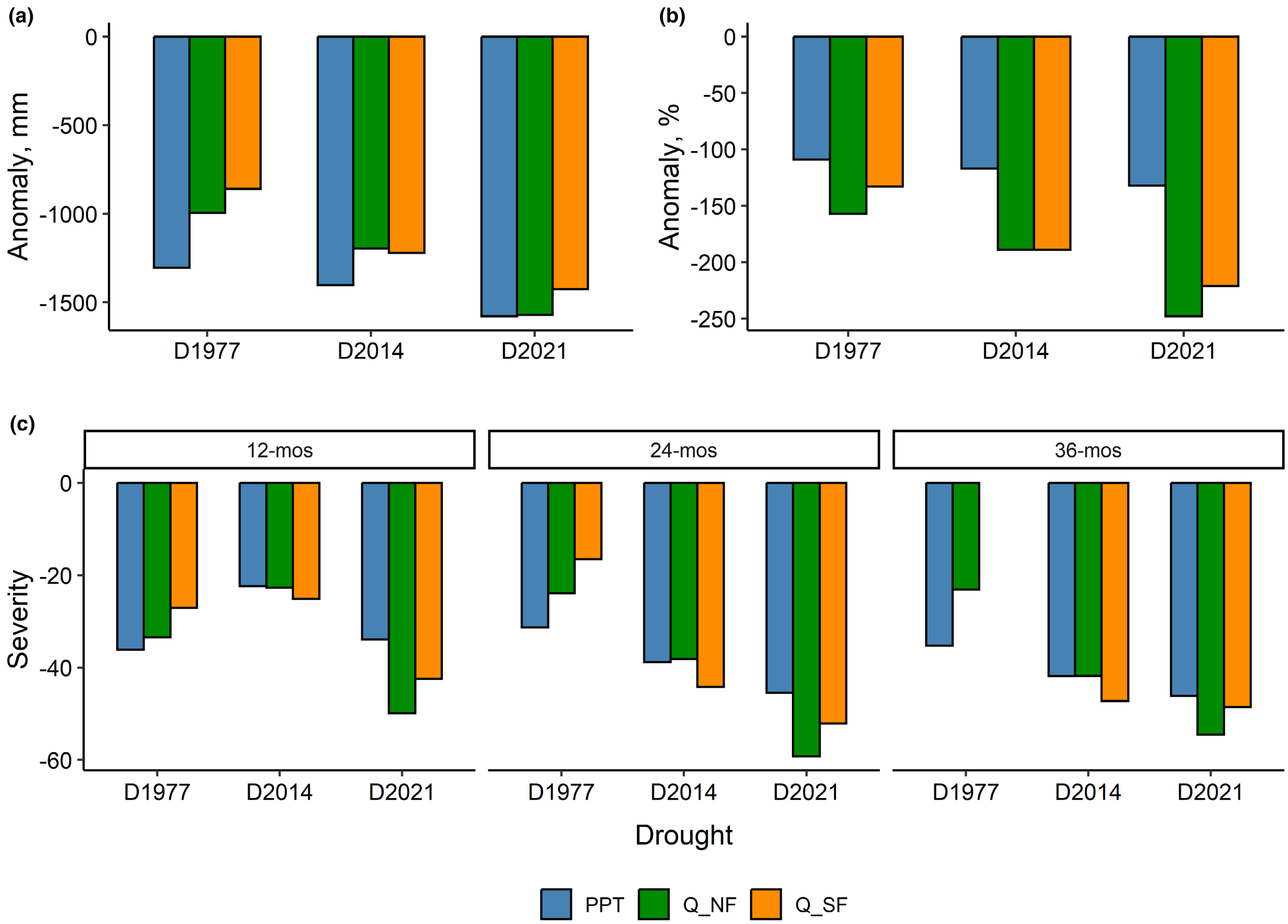

FIGURE 5 Maximum accumulated monthly anomaly for precipitation (PPT), NF streamflow (Q_NF), and SF streamflow (Q_SF) in absolute terms (a) and as percent of annual mean (b) during 1977 (D1977), 2014 (D2014), and 2021 (D2021) drought events. Mean annual values for the reference period (1962–1984) were 1198 mm, 633 mm, and 645 mm for precipitation, NF streamflow, and SF streamflow, respectively. (c) Drought severity using 12-, 24-, and 36-month integrations for SPI (PPT) and NF SRI (Q_NF) and SF SRI (Q_SF) during the three drought events.

in the amount of seasonal precipitation antecedent to the first SPQ_{10} ($t_{(59)}=0.197$, $p=0.013$). Additional trends were also identified for several hydrologic and temperature variables used in later model development (Table 4).

From 1985 to 2022, mean annual precipitation was 6% lower than the 1962–1984 NF pretreatment reference period used to determine monthly means, although this difference was not statistically significant. However, fall precipitation and streamflow declines were significant. Fall precipitation declined by one-third (100 mm) as compared to the reference period amount (305 mm). Similarly, fall streamflow declined by 36 mm on the NF and 54 mm on the SF as compared to the reference values of 54 and 76 mm, respectively. The first 10% exceedance flow (Q_{10}) typically occurred in late November during the reference period but was delayed to mid-December during the latter period for both forks (NF: from November 28 to December 18; SF: from November 25 to December 17).

SF streamflow declines were more pronounced than NF (Figure 3b). No difference in trend was detected between the accumulated precipitation anomaly (AMPA) and the NF streamflow anomaly (AMNA), whereas the SF anomaly (AMSA) differed from both AMPA ($p<0.0001$) and AMNA ($p=0.015$).

3.4 | Logging effects

A comparison of 5-year post-harvest annual flow enhancements relative to the unharvested catchment indicated that the largest increases occurred after the first experimental harvest and the smallest occurred after the third harvest (Table 5; Figure 6). The mean increase after the first experimental harvest in the SF removed 62% of the stand volume was 38%. The mean PPT_{12} for this 5-year period (1974–1978) was neutral (−0.1). After the harvest was completed in the SF in 1973, SF flows remained elevated relative to NF until 1990, when the pattern

TABLE 4 Mann–Kendall trend analysis results for precipitation and streamflow time series; *p*-value is for 1 − sided test, degrees of freedom (df), and trend. Variables are defined in Table 2.

Variable	*p*-value	df	τ	Trend
PPT	0.205	60		NS
SEP–NOV	0.027	60	−0.17	Decreasing
NOV	0.039	60	−1.56	Decreasing
AUG	0.001	60	−0.30	Decreasing
NFmm	0.069	60		NS
SEP–NOV	0.013	60	−0.20	Decreasing
NFrr	0.042	59	−0.15	Decreasing
NFcent	0.034	59	0.16	Increasing
Ndayz	0.014	58	0.20	Increasing
NdayzR	0.002	58	0.27	Increasing
NFT_{gsm}	0.001	60	0.29	Increasing
NFT_{spm}	0.001	60	0.28	Increasing
Gw_{min}	0.007	14	−0.49	Decreasing
SFmm	0.021	59	−0.18	Decreasing
SEP–NOV	0.001	60	−0.29	Decreasing
OCT–DEC	0.047	60	−0.15	Decreasing
SFrr	0.001	59	−0.27	Decreasing
SFcent	0.029	59	0.17	Increasing
Sdayz	0.007	59	0.22	Increasing
SdayzR	0.007	59	0.27	Increasing
SPQ10	0.013	59	0.20	Increasing
SF_{12}	0.019	59	−0.19	Decreasing
SF_{36}	0.010	57	−0.21	Decreasing
SFaa	0.021	59	−0.18	Decreasing
SFS_{fw}	0.006	59	0.23	Increasing
SFS_{w}	0.004	59	0.24	Increasing
SFT_{gsm}	0.001	59	0.28	Increasing
SFT_{spm}	0.002	59	0.25	Increasing
$SPQ_{10}adj$	0.009	59	0.21	Increasing

TABLE 5 Harvest intensity for three experimental treatments with 5-year post-harvest drought intensity and streamflow response.

	Experiment 1: 1971–1973	Experiment 2: 1989–1992	Experiment 3: 2017–2019
Watershed	SF	NF	SF
Stand reduction, %	62	37	32
Harvest method	Selection	Partial clear-cut	Selection, variable retention
PPT_{12}, 5-year mean	−0.1	0.5	−1.1[a]
Flow increase, mm	605	292	181[a]
Flow increase, %	38	10	31[a]
Maximum 1-year increase, %	106	17	53

[a]4-year post-harvest period for Experiment 3.

reversed due to NF harvest response. In contrast, the post-harvest period following the second experimental harvest, which used clear-cutting to remove 37% of the stand volume of the NF, was relatively wet, with a mean PPT_{12} of 0.5 (1993–1997). The flow enhancement for this period averaged just 10%, and the elevated flows in the NF persisted until 2013 (Figure 6b). During the 4-year period following the most

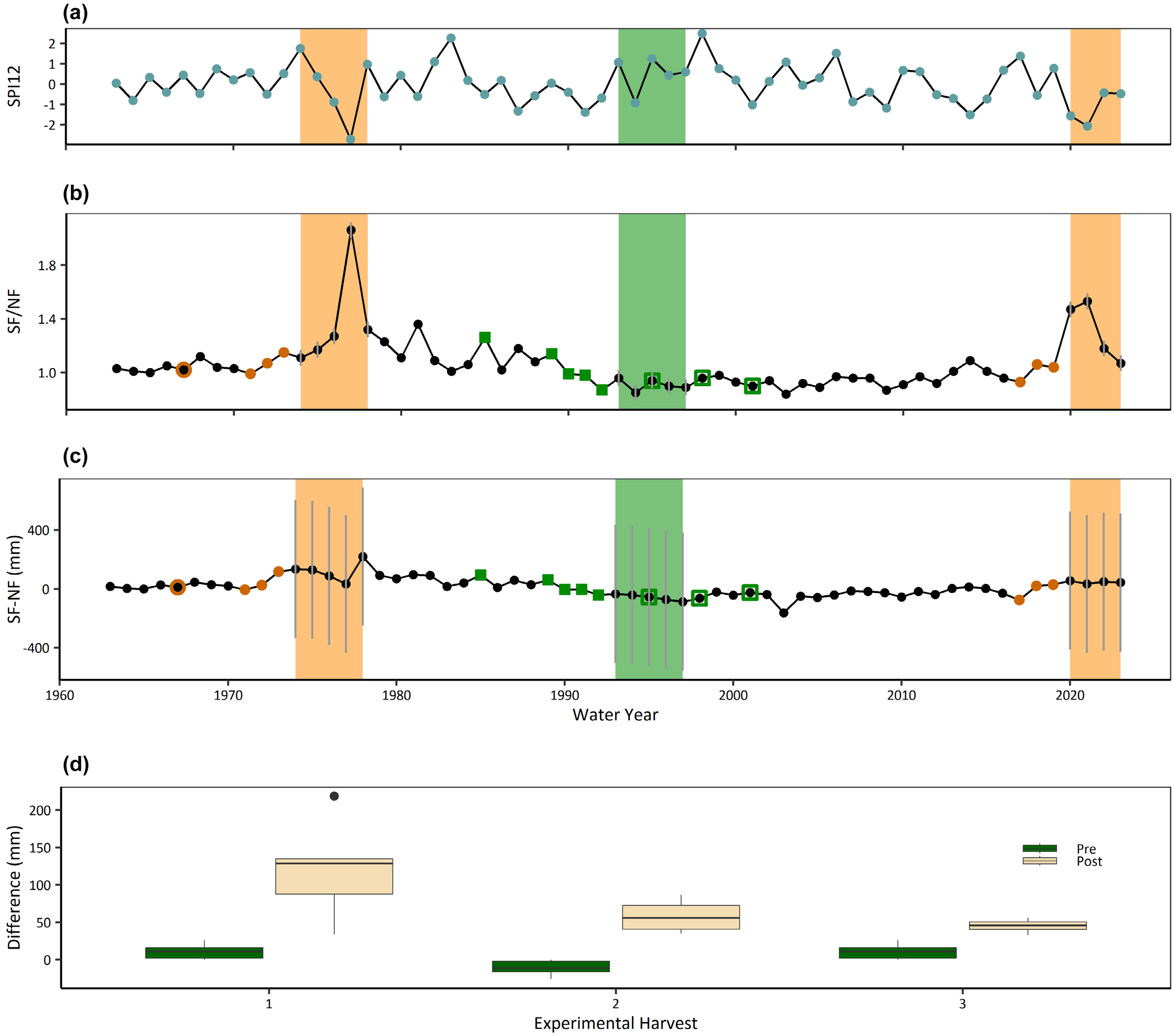

FIGURE 6 (a) September drought index for precipitation (SPI_{12}), (b) ratio of SF streamflow (SF) to NF streamflow (NF), (c) SF streamflow minus NF streamflow with prediction limits based on water years 1964 to 1967 pre-harvest period, and (d) boxplots of the differences between treated watershed streamflow and reference watershed streamflow (treated—reference) in the 5 years pre-harvest and the 5 years post-harvest for the three experimental harvests. Only 4 years are shown for the most recent harvest. Boxplots show medians as lines, 1st and 3rd quartiles as boxes, and 1.5 times the interquartile range as whiskers. In (b) and (c), logging years are shown as orange circles (SF) and green squares (NF), with unfilled symbols indicating low-intensity vegetation reductions associated with road construction (SF) and pre-commercial thinning (NF); background shading indicates post-harvest periods (1974–1978, 1993–1997, and 2020–2023).

recent experimental harvest in the SF (32% stand reduction by selection harvest), conditions were drier with a mean PPT_{12} of −1.1 (2020–2023). The mean flow enhancement in the SF during this period was 31%. Across the three harvests, the largest single-year proportional flow enhancements were observed in severe drought years 1977 (106% increase) and 2021 (53% increase) on SF, and mild drought year 1994 (17% increase) on NF. In absolute terms, the 5-year increase following the first experimental harvest in the SF (605 mm) was about double that following the experimental harvest in the NF (292 mm) (Figure 6c). In the SF, the basal area reduction during the 2017–2019 experimental harvest was about half that of the 1970s experimental harvest, which may have contributed to the smaller flow enhancement of 181 mm during the 4-year post-harvest period.

At the monthly scale, the largest difference between the SF and NF streamflow (82 mm) was observed in December 1977 (SPI_{12} = −1.1), when renewed rainfall began to alleviate the D1977 meteorological drought. After the NF harvest was completed in 1992, the largest difference between NF and SF (52 mm) was not observed until December 2002 (SPI_{12} = 0.2)—less than 2 years after pre-commercial thinning was completed and following the mild drought year of 2001 (PPT_{12} = −1). After the 2017–2019 experimental harvest in the SF, the largest difference between the SF and NF monthly discharge (23 mm) was observed in December 2022 ($SPI_{12}=-1.0$) immediately following the maximum drought anomaly and as this most recent and most severe drought was beginning to subside. In all three cases, these maximum post-harvest increases in streamflow occurred after drought years ($PPT_{12} < -1$).

3.5 | Models

3.5.1 | Annual flow anomalies

Correlation analysis indicated hydrologic variables were generally the most influential predictors of observed differences between the rainfall and runoff anomalies (Ndiff and Sdiff) (Table 6). For the NF, the first four highly significant variables ($n=51$, $p<0.001$) reflect replenishment of subsurface storage (NFS_{fw}), spring water balance (NFB_{sp}), annual moisture stress (accumulated for months where PPT < PET), and dry season PET in excess of precipitation ($NFET_s$)—all derived in part from precipitation and flow. A second tier of significant correlations ($n=51$, $p<0.005$) included the three residual tree ring growth indices with climatic persistence influence removed, indicative of growth conditions in nearby coast redwood plots (TR_{res}, FWP_{res}, and NR_{res}). For the SF, the same four hydrologic parameters along with harvest impact (SFHi) were highly significant ($n=51$, $p<0.001$). The second tier of significantly correlated variables included WY, fall replenishment of subsurface storage (SFS_f), a tree ring width growth index (TRres), and stand density index (SF_SDI_{max}). In sum, 16 NF and 24 SF candidate variables were significantly correlated with the difference between precipitation and flow anomalies (Ndiff and Sdiff).

Linear models were developed to explore variations in Ndiff and Sdiff. Seasonal water balance and storage components with standardized coefficients were useful in identifying where in the annual cycle these differences were originating and explaining nearly all of the variation in NF and SF (adjusted $R^2=0.99$). Fall storage replenishment (NFS_f) and water balance (SFB_f) were the most influential predictors of overall differences between precipitation and flow anomalies (Ndiff and Sdiff) (Table 7).

3.5.2 | Ten percent exceedance flows (Q_{10})

Flow duration analysis of NF mean daily flow yielded a Q_{10} value of 0.213 m^3/s (higher than the SF Q_{10} value of 0.183 m^3/s). During the 60-year record, NF did not attain Q_{10} in WY 1977, and neither stream attained Q_{10} in WY 2021. In the remaining years, the initial Q_{10} typically occurred in November or December but occurred as early as late October and as late as early March. Cumulative precipitation preceding the first Q_{10} flow for the NF (NPQ_{10}) averaged 298 mm and ranged from 163 to 492 mm, while the mean for the SPQ_{10} was 274 mm and ranged from 129 to 476 mm (Figure 7b). The mean SPQ_{10} was lower than the NPQ_{10} ($t_{(58)}=3.03$, $p=0.004$), as was the mean number of days to Q_{10} (70 for SF vs. 72 for NF; $t_{(58)}=2.19$, $p=0.03$).

Drought significantly delayed or pre-empted the initial Q_{10} (Figure 7a). During drought conditions ($PPT_{12} < -1$), the mean number of days to the first Q_{10} of the WY (128 on NF and 120 on SF) was about twice that of normal years ($-1 < PPT_{12} < 1$) (67 on the NF and 65 on the SF; $p<0.0001$), and the difference was even greater when compared to wet conditions ($PTT_{12} > 1$).

The length of the wet-up season and the number of rainy days preceding Q_{10} were highly correlated with NPQ_{10} and SPQ_{10} ($r > 0.68$, $p<0.0001$), thus these were excluded from our regression models. Instead, we characterized the distribution of antecedent precipitation using the ratio of rainy to total days prior to the initial Q_{10} (DR). For NF, the most parsimonious model included DR, NF basal area (NFBAa), and prior summer streamflow (NFLFpy) (adjusted $R^2=0.20$, $p=0.0025$) (Table 8). Drought year 2014 exhibited the largest standardized residual for $NPQ_{10}adj$ in this model. For SF, the fitted model also included DR and prior summer streamflow (SFLFpy), as well as prior year drought index ($PPT_{12}py$) and prior year growing season mean air temperature ($SFT_{gsm}py$), reflecting additional climatic effects. The largest standardized residuals from this model occurred in drier years 2009, 2020, 1994, and 1992, suggesting a far higher SPQ_{10} during severe drought. Despite the suggested influence of prior year drought on SPQ_{10}, no significant difference was detected among mean SPQ_{10} following dry ($PPT_{12} < -1$), wet ($PPT_{12} > 1$), or normal water years ($p>0.05$).

3.5.3 | Dynamic storage: Fall/winter

Dynamic storage estimates for fall and winter (NfS_{fw} and SFS_{fw}) were the most correlated to the differences between precipitation and flow anomalies (Ndiff and Sdiff). Notably, the fall surplus (NfS_f and SFS_f) was better correlated to this difference than the winter surplus (NFS_w and SFS_w) (Table 6). These parameters account for most of the variation in the annual difference between rainfall and runoff anomalies and as expected, were significant hydrologic predictors in the multiple regressions used to explore differences between precipitation and flow anomalies (Table 7). These regression results merely highlight the relative seasonal contributions to the overall differences and led us to focus our analysis

TABLE 6 Pearson's correlation coefficients (*r*) and *p*-values for candidate variables screened for modeling the difference between the precipitation and flow anomaly for the NF (Ndiff) and SF (Sdiff). Variables are ordered by the sum of the *p*-values for both forks ($n=51$ except where noted). Bold indicates significant correlations ($p<0.05$).

Variable	*r* NF	*p*-value NF	*r* SF	*p*-value SF
Fall + winter surplus (NFS_{fw}, SFS_{fw})	**0.75**	<0.0001	**0.84**	<0.0001
Spring water balance (NFB_{sp}, SFB_{sp})	**0.51**	<0.0001	**0.66**	<0.0001
Moisture stress (NFMS, SFMS)	**−0.61**	<0.0001	**−0.47**	0.0004
Summer evapotranspiration ($NFET_s$, $SFET_s$)	**0.45**	0.0009	**0.49**	0.0003
Average of FWP_{res} and NR_{res} (TR_{res})	**0.43**	0.0015	**0.42**	0.0024
Fall water balance (NFB_f, SFB_f)	**0.36**	0.0045	**0.47**	0.0047
Fritz Wonder Plot, residual incremental growth (FWP_{res})	**0.42**	0.0024	**0.41**	0.0029
Fall surplus (NFS_f, SFS_f)	**0.37**	0.0076	**0.46**	0.0007
Navarro Redwoods, residual incremental growth (NR_{res})	**0.39**	0.0044	**0.37**	0.0081
12-month SPI (PPT_{12})	**0.36**	0.0091	**0.34**	0.0137
Mean of FWP_{std} and NR_{std} (TR_{std})	**0.35**	0.0128	**0.33**	0.0176
Annual precipitation (PPTmm)	**0.34**	0.0138	**0.33**	0.0188
Precipitation annual anomaly (PPTaa)	**0.34**	0.014	**0.33**	0.0188
Summer surplus (NFS_s, SFS_s)	**0.31**	0.0271	**0.37**	0.0068
Fritz Wonder Plot, standardized incremental growth (FWP_{std})	**0.34**	0.0143	**0.32**	0.023
Navarro Redwoods, standardized incremental growth (NR_{std})	**0.3**	0.0323	**0.3**	0.0349
Winter surplus (NFS_{fw}, SFS_{fw})	0.2	0.1574	**0.35**	0.0131
Consecutive year of drought per SPI_{12} (DY12)	−0.22	0.097	−0.21	0.0995
36-month SRI (NF_{36}, SF_{36})	−0.19	0.1728	−0.25	0.0804
Winter water balance (NFB_w, SFB_w)	0.16	0.2403	**0.3**	0.0203
Summer water balance (NFB_{su}, SFB_{su})	0.17	0.1891	−0.15	0.2684
Spring air temperature (NFT_{spm}, SFT_{spm})	0.09	0.5215	**0.39**	0.0048
Harvest impact (NFHi, SFHi)	0.09	0.5271	**−0.6**	<0.0001
Stand Density Index (NF_SDI_{max}, SF_SDI_{max})	0.07	0.6167	**0.41**	0.0025
Water year (WY)	0.07	0.6469	**0.47**	0.0005
Growing season air temperature (NFT_{gsm}, SFT_{gsm})	0.06	0.6771	**0.38**	0.006
12-month SRI (NF_{12}, SF_{12})	0.19	0.1937	0.09	0.5458
24-month SRI (NF_{24}, SF_{24})	−0.11	0.4564	−0.15	0.2958
Basal area (NFBAa, SFBAa)	0.04	0.795	**0.33**	0.0185
Runoff ratio (NFrr, SFrr)	−0.04	0.8019	−0.21	0.1477

TABLE 6 (Continued)

	r	*p*-value	*r*	*p*-value
Variable	NF		SF	
Streamflow annual anomaly (NFaa, Sfaa)	0.13	0.3814	0.04	0.7629
Streamflow (NFmm, SFmm)	0.13	0.3816	0.04	0.7658
24-month SPI (PPT_{24})	0.02	0.8934	0.1	0.4969
36-month SPI (PPT_{36})	−0.08	0.5768	0.01	0.9232
Basal area in uncut plots (UnBAa)	0.09	0.5388		
Annual minimum groundwater depth (GW_{min}); $n=14$	−0.21	0.586		

TABLE 7 Regression results for difference between annual precipitation and flow anomalies for NF (Ndiff) and SF (Sdiff) using standardized seasonal water balance-based predictors. Abbreviations are defined in Table 2.

Response	Predictor	Coeff.	Std. error	*p*-value	df	Adj. R^2
Ndiff	Full model		1.34	<0.0001	55	0.999
	(Intercept)	3.38	0.18	<0.0001	1	
	NFS_f	90.5	0.27	<0.0001	1	
	NFS_w	80.7	0.27	<0.0001	1	
	NFB_{sp}	47.6	0.18	<0.0001	1	
	NFB_{su}	20.0	0.18	<0.0001	1	
Sdiff	Full model		1.32	<0.0001	55	0.999
	(Intercept)	4.17	0.17	<0.0001	1	
	SFB_f	87.39	0.22	<0.0001	1	
	SFB_w	76.42	0.22	<0.0001	1	
	SFB_{sp}	50.84	0.17	<0.0001	1	
	SFB_{su}	24.99	0.19	<0.0001	1	

on factors influencing variations in fall dynamic storage. Multiple regression analyses of the factors affecting fall replenishment of subsurface moisture deficit indicated prior year conditions were influential (Table 9). For the NF model, the prior year Navarro Redwoods radial growth index (NR_{res}py) and prior year drought conditions (NF_{24}py and NF_{36}py) were the most useful predictors (adjusted $R^2=0.27$, $p=0.0005$), while for SF the WY and stand density index (SF_SDI_{max}) added to the predictive ability of the overall model (adjusted $R^2=0.31$, $p=0.0006$).

Subsetting the data by harvest impact yielded unique and contrasting models (Table 9). For NF "non-logging" years (herein defined as pre-harvest and greater than 10 years post-harvest), prior year moisture stress (NFMSpy) and prior year summer flow (NFLFpy) enhanced the model's predictive ability (adjusted $R^2=0.44$, $p<0.0001$). For those years with harvest impact, the expanded NF model (adjusted $R^2=0.93$, $p=0.0003$) included stand density index (NF_SDI_{max}), basal area in the unharvested areas of the watershed (UnBAa), consecutive year of drought (DY12py), and harvest impact (NFHi) in addition to the prior year SPI (PPT_{12}py) and prior year precipitation (PPTpy). For SF, the simplified model for "non-logging" years included only the Navarro Redwoods growth index (NR_{std}py) and explained a minimal amount of the variability in fall surplus (adjusted $R^2=0.17$, $p=0.0059$). The SF harvest impact model had greater predictive ability (adjusted $R^2=0.92$, $p<0.0001$) and included the average radial growth index (TR_{std}) and three prior year predictors: 36-month SRI (SF_{36}py), summer surplus precipitation in excess of PET (SFS_spy), and 24-month SPI (PPT_{24}py).

4 | DISCUSSION

4.1 | Timing and magnitude of meteorologic and streamflow drought

The three episodes of most severe drought in the 60-year record were sequentially longer and more severe. Hydrologically, the longer droughts of the 21st Century were more severe and resulted in proportionately larger anomalies (Table 3; Figure 5). The earliest severe drought in our record (D1977, 1976–1977) was short-lived and ameliorated more quickly than the subsequent droughts. Above-average precipitation during

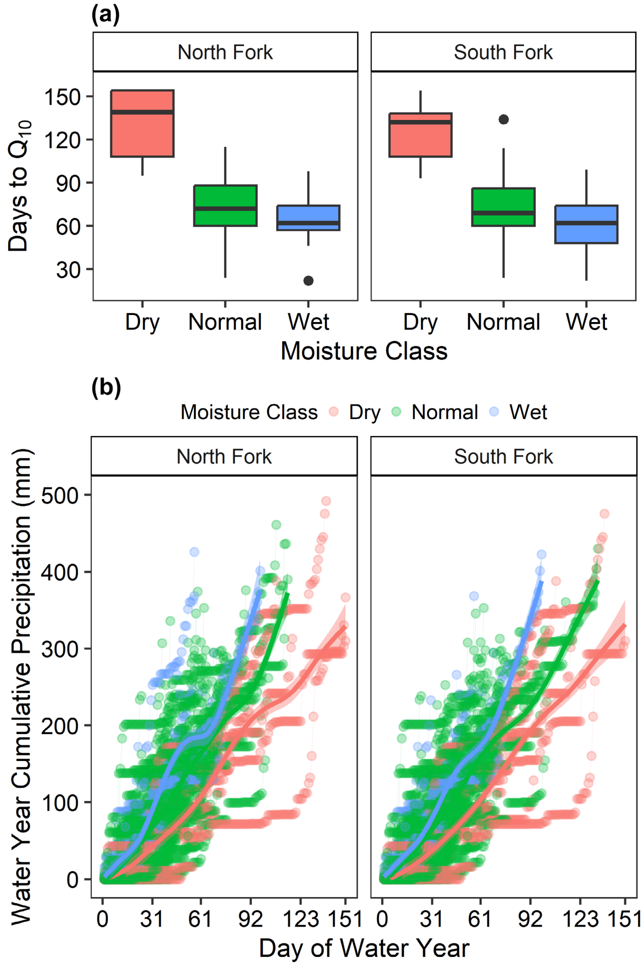

FIGURE 7 (a) Number of days preceding the first 10% exceedance flow of the year (Q_{10}) for North Fork (NF) and South Fork (SF) following dry ($PPT_{12} < -1$; red shading or symbols), normal ($-1 \le PPT_{12} \le 1$; green shading or symbols), and wet ($PPT_{12} > 1$; blue shading or symbols) years. (b) Cumulative precipitation prior to the first Q_{10} for each water year for the NF and SF. Q_{10} was not achieved in the NF in WY 1977 or in either fork in WY 2021, and these years are excluded.

TABLE 8 Regression results for precipitation preceding the first Q_{10} flow of each water year for North Fork (NF; NPQ_{10}adj) and South Fork (SF; SPQ_{10}adj) using standardized predictors. Abbreviations are defined in Table 2. Predictors derived from prior water year end with a "py". Marginal adjusted R^2 values in parentheses represent adjusted R^2 with incremental inclusion of additional variable.

Response	Predictor	Coeff.	Std. error	*p*-value	df	Adj. R^2
log(NPQ_{10}adj)	Full model		0.215	0.0023	50	0.205
	(Intercept)	5.646	0.029	<0.0001	1	
	DR	0.086	0.030	0.006	1	(0.103)
	NFBAa	−0.087	0.032	0.010	1	(0.147)
	NFLFpy	−0.068	0.032	0.041	1	(0.205)
log(SPQ_{10}adj)	Full model		0.212	<0.0001	50	0.382
	(Intercept)	5.543	0.029	<0.0001	1	
	SFLFpy	−0.190	0.046	0.0002	1	(0.167)
	SFT_{gsm}py	0.082	0.029	0.0068	1	(0.271)
	SPI_{12}py	0.098	0.046	0.0387	1	(0.346)
	DR	0.061	0.030	0.0501	1	(0.382)

the 3 years prior to and first year after this drought contributed to the relatively rapid recovery. Watershed "memory" of this drought, as measured by the persistence metric, was negligible on the recently logged SF, but 19 months on the NF (per NF_{12}). Because of the relatively brief duration of this drought, the 12-month SPI and SRI were most useful for meteorologic-to-streamflow comparisons, while intensity as

TABLE 9 Regression results for dynamic storage fall replenishment for North Fork (NF; NFS_f) and South Fork (SF; SFS_f) for all years, non-logging years (pre-harvest and greater than 10 years post-harvest), and post-logging years (within 10-year post-harvest period) using standardized predictors. Abbreviations are defined in Table 2. Predictors derived from prior water year end with a "py".

Response	Predictor	Coeff.	Std. error	*p*-Value	df	Adj. R^2
NFS_f	Full model		79.4	0.0005	47	0.268
	(Intercept)	315.6	11.1	<0.0001	1	
	NR_{res}py	−52.8	12.2	<0.0001	1	
	NF_{24}py	68.7	23.3	0.0050	1	
	NF_{36}py	−49.6	22.4	0.0316	1	
NFS_f (non-logging)	Full model		67.1	0.0003	31	0.436
	(Intercept)	332.4	11.0	0.0056	1	
	NFMSpy	41.7	14.0	0.0007	1	
	NR_{res}py	−59.1	15.8	0.0018	1	
	PPT_{24}py	70.6	20.6	0.0056	1	
	NF_{36}py	−55.1	18.5	0.0511	1	
	NFLFpy	36.1	17.8	0.0056	1	
NFS_f (post-logging)	Full model		23.1	<0.0001	7	0.934
	(Intercept)	270.9	6.2	<0.0001	1	
	NF_SDI_{max}	192.1	20.3	<0.0001	1	
	UnBAa	−149.7	18.1	0.0001	1	
	DY12py	85.5	10.0	0.0001	1	
	PPT_{12}py	310.4	67.2	0.002	1	
	PPTpy	−313.0	64.8	0.002	1	
	NFHi	−37.1	9.6	0.006	1	
SFS_f	Full model		75	0.0006	45	0.306
	(Intercept)	−22,819	7913	0.0060	1	
	NR_{res}py	−526.6	142.6	0.0006	1	
	WY	12.24	4.12	0.0047	1	
	SF_SDI_{max}	−1997	749	0.0106	1	
	SF_{24}py	70.18	22.82	0.0036	1	
	SF_{36}py	−51.77	21.89	0.0224	1	
SFS_f (non-logging)	Full model		79.3	0.0059	35	0.174
	(Intercept)	313.4	13.0	<0.0001	1	
	NR_{std}py	−38.77	13.2	0.0059	1	
SFS_f (post-logging)	Full model		25.2	<0.0001	9	0.924
	(Intercept)	267.3	6.74	<0.0001	1	
	TR_{std}	36.51	8.07	0.0014	1	
	PPT_{24}py	46.07	10.4	0.0016	1	
	SF_{36}py	−83.90	10.3	<0.0001	1	
	SfS_spy	−57.34	8.0	<0.0001	1	

indicated by the 36-month indices did not meet our definition of severe streamflow drought. In contrast, the intensity and severity of the 21st Century droughts were more evident in the 24- and 36-month indices. These streamflow droughts showed greater severity and intensity than the meteorologic drought and longer watershed "memory". In the case of D2014, precipitation deficits spanned 4 years (2012–2015), followed by 3 years of above-normal precipitation in the subsequent 4-year period before the onset of D2021 in 2020. Precipitation during this period of non-drought was insufficient to ameliorate the deficit that accrued during D2014; hence, recovery was not observed. This appears to have contributed to the more severe and intense streamflow drought response, particularly on NF, during D2021. The latter drought has not ameliorated, although above-normal precipitation in 2023 ended the period of severe drought.

Our analysis highlights the utility and limitations of the SPI. Selection of an appropriate integration period is key to making relevant comparisons. Our approach was to first evaluate the duration of the drought anomaly using the accumulated monthly precipitation anomaly and then select an integration interval of sufficient length to capture the drought development period. In our analysis, the 12-month index was most relevant to D1977 comparisons, while the 24- and 36-month indices were more useful for comparing the lengthier droughts (D2014 and D2021). Additionally, the SPI does not account for temperature and plant water use. The Standardized Precipitation and Evapotranspiration Index (SPEI) accounts for both precipitation and PET and was specifically developed for studies of the impacts of global warming on drought severity (Vicente-Serrano et al., 2010). SPEI may be a useful drought metric for exploring temperature-induced changes in hydrological drought, particularly during periods of low flow.

4.2 | Streamflow responses to timber harvest and recovery

Post-harvest streamflow responses likely reflect differences in harvest intensity and silvicultural methods, as well as year-to-year variations in precipitation (Figure 6). Differences between the NF and SF runoff indices provide evidence of post-harvest flow enhancement due to reduced evapotranspiration and interception (Figure 3a). These differences are consistent with earlier conclusions of increased annual yields, peak flows, and summer low flows after the first two experimental harvests (Keppeler, 1998; Keppeler et al., 2009; Lewis et al., 2001). During the initial post-harvest decade, annual yield increases were similar when calculated per unit of equivalent clear-cut area (Keppeler et al., 2009), but recovery trajectories differed between the SF selection harvest (67% basal area removal) and partially clear-cut NF (50% basal area removal) with variations explained in part by differences in silvicultural methods. Low flow responses were more unique. Reid (2012) reported that summer low flow increases disappeared by 7 years after the completion of the SF harvest and then declined below pretreatment levels until 30 years post-harvest, while on NF summer low flows remained higher than expected for at least 15 years post-harvest. This suggests that residual trees in the selection- harvested SF stands benefitted from reduced competition for soil moisture at the local scale, a result consistent with the findings of Bart et al. (2021). In contrast, trees remaining after clear-cutting were mostly in unthinned patches or lightly thinned riparian areas, and therefore did not have access to more elevated subsurface moisture in harvested portions of the watershed. Herbicide application and pre-commercial thinning in NF clear-cuts further suppressed revegetation, which would increase soil moisture surpluses. Hypothetically, this surplus moisture enhanced groundwater recharge in clear-cut areas and resulted in more persistent summer flow enhancements in the partially clear-cut NF.

During wet years, transpiration accounts for a smaller fraction of the total water balance, thus streamflow differences between logged and unlogged catchments are proportionately smaller (Keppeler et al., 2009; Reid & Lewis, 2011). In contrast, during drought years, transpiration may account for as much as 90% of the rainfall, so reduced transpiration in logged areas—or enhanced transpiration in rapidly regrowing areas (Coble et al., 2020; Gronsdahl et al., 2019; Perry & Jones, 2017)—can lead to large differences in hydrologic response relative to watersheds supporting mature forest. Thus, the subsequent reduction in late summer flows reported by Reid (2012) and attributed to enhanced evapotranspiration during regrowth may have contributed to the greater severity and intensity of D2014 on SF relative to NF.

Outside of harvesting, road building can have significant and enduring impacts on streamflow dynamics (Jones, 2000; Jones & Grant, 1996; King & Tennyson, 1984; Lamarche & Lettenmaier, 2001). Our results suggest the same in that SF flows remained elevated relative to NF when NF logging was implemented in 1985 (Figure 6). Overall, SF had lower cumulative precipitation preceding the 10% exceedance flow (SPQ_{10}), as well as a shorter length of the wet season (Sdayz) relative to NF (Ndayz), which may reflect differences in the area and distribution of roads and skid trails. The initial SF harvest operations included 4.6 km of riparian road construction (1967), and additional roads and skid trails occupied 15% of the watershed area. Since the 1970s era, tractor logging, natural processes, and active management (road decommissioning and erosion control measures implemented in conjunction with the 2017–2019 experimental harvest in the SF) have disrupted surface flowpaths and gradually enhanced natural infiltration. Overland flow is still observed on the roads, landings, and skid trails that have not been removed, and direct routing of surface water to SF channel can occur. In contrast, new road and landing construction accounted for only 3% of the NF area during the second harvest experiment and less than 2% of SF area during the third harvest experiment. Roads were installed mostly near ridges for the latter two harvests. As is typical in forested areas, overland flow is rarely observed in areas not compacted by heavy equipment, and runoff generated along compacted surfaces typically infiltrates before reaching the channel network. Thus, road building may explain the lower SPQ_{10} (Figure 7) and the influence of water year (WY) as a predictor of fall storage replenishment (Table 9).

4.3 | Storage dynamics and drought

Variations in dynamic storage account for most of the difference between the precipitation and flow anomalies observed in our analysis. In the wet winter, dry summer Mediterranean climate typical of the Northern California Coast Range, there is minimal soil moisture storage at the end of the summer season and early fall. Dralle et al. (2018) suggest that dynamic storage in the subsurface critical zone (fresh bedrock to soil surface) can be divided into two pools: direct (hydraulically coupled) and indirect (decoupled subsurface storage). Direct storage, commonly interpreted as hillslope groundwater, drives streamflow generation, while indirect storage (unsaturated storage in soil and weathered bedrock) equates to plant-available water in the unsaturated zone and accounts for most of total dynamic storage in a catchment. Indirect storage exhibits less inter-annual variability and is difficult to measure without intensive field effort. Applying this conceptual framework to our data, we estimate dynamic storage of 440–570 mm—a "storage capacity limited" condition wherein annual precipitation typically exceeds this dynamic storage capacity (Figure S3). This storage capacity is replenished in all but the most extreme drought years (1977 and 2021, for example), as fall and winter rains increase moisture content in both the soil and saprolite and contribute to the water table and stream via saturated and preferential flow. During a March 2021 subsurface sampling campaign coincident with near-peak drought ($SPI_{12}=-1.91$), drier conditions were observed in the saprolite (2–3 m depth) relative to the upper meter of soil, indicating a lack of uniform saturation and decoupling of stored moisture from the stream (unpublished data).

In a recent analysis of SF hillslopes, quick dry to wet transitions in soil moisture and high temporal variability at 1-m soil depth during both wet and dry seasons were attributed in part to sandy soil textures (Dymond, Wagenbrenner, et al., 2021). This was true both in drought ($PPT_{12}=-1.4$) and non-drought ($PPT_{12}=1.3$) conditions during that study. On average, soils attained mean wet season moisture levels by late November or December after ≈330 mm of precipitation, and there was variability across the hillslope (Dymond, Wagenbrenner, et al., 2021). At Caspar Creek, rain event water may drain directly to shallow groundwater, or it may flow via preferential flow pathways that bypass much of the unsaturated soil matrix (Keppeler & Brown, 1998). Hahm, Rempe, et al. (2019) demonstrated that dynamic storage capacity scales with the combined depth of weathered bedrock and saprolite at their nearby Northern Coast Ranges field site. Depending on hillslope position, measured depth of fractured bedrock ranges from 3 to 8 m at our sites. The amount of event water that is absorbed versus transmitted through this deep profile in varying moisture states is unknown but may account for variations in dynamic storage that in turn govern the difference between precipitation and streamflow characterized in our long-term drought responses.

In the hillslope soil moisture study in the SF, the slow transition from wet to dry soil moisture states was similar in 2016 and 2017, although May SPI_{12} was lower in 2016 (0.71) than 2017 (1.35) (Dymond, Wagenbrenner, et al., 2021). May SPI_{36} indicated a lingering drought in 2016 (−0.71) versus 2017 (0.76), but this appears to have been inconsequential in terms of soil moisture recession. As the wet season ends, groundwater recedes to sustain only minimal streamflow, and May through October streamflow averages only 5% of annual runoff. Indirect storage in the vadose zone and weathered bedrock remain available to transpiring plants during the lengthy dry season. This supports the idea that seasonal precipitation patterns primarily control the soil moisture, irrespective of drought condition (Hahm et al., 2022). This may not be the case deeper in the critical zone. May to October piezometer readings at SF ridge positions indicated higher groundwater levels in 2017 compared to 2016, whereas riparian piezometer levels across these 2 years were similar (unpublished data). This adds credence to the hypothesis that subsurface storage in upslope positions is largely decoupled from the stream, except in very dry conditions when precipitation is insufficient to ameliorate the subsurface deficit (Dralle et al., 2018). Minimum groundwater levels measured in a NF swale (2007–2022) were consistently 2–3 m below the ground surface, a depth approximating the maximum coast redwood rooting depth (Hermann & Lavender, 1990). This subsurface reservoir appears to contribute to streamflow via soil pipeflow when pipe source area is locally saturated (Ziemer & Albright, 1987) as well as transpiration (unpublished data). Preliminary analysis of this well data (2007–2022) indicates that both PPT_{24} and NF_{24} were significant predictors (adj. $R^2=0.41$, df = 14, $p=0.017$) of minimum groundwater level at this location.

4.4 | Biotic and climatic influences on dynamic storage

Inter-annual variations observed in dynamic storage appear to be due to biotic and climatic factors, including the distribution of precipitation throughout the year. Our models indicate that both growth conditions (as indexed by radial increment growth) and prior year SRI (24 and 36 months) influence the magnitude of subsurface storage deficits as evidenced by fall replenishment. Thus, we infer that these deficits reflect prior drought and pluvial conditions, despite storage capacity limitations that constrain the maximum storage at any given time. Moisture stress is a significant predictor in our regression analyses, indicating the influence of intra-annual depletion and replenishment of storage (Table 9). Defined as the sum of monthly PET in excess of PPT, this variable captures the effects of more transient winter deficits. For example, although winter PET is relatively low, a transient storage deficit may develop during a dry winter month, contributing to higher moisture stress. Thus, storage is depleted and later replenished when precipitation in excess of PET occurs in ensuing months. In contrast, surplus summer precipitation (in excess of PET) may partially alleviate some of the deficit developing over the growing season, thereby reducing the cumulative end-of-season deficit and subsequent fall replenishment.

Our results show weak but statistically significant correlations between tree growth (as measured via radial increment growth at both the Fritz Wonder and Navarro Redwoods plots) and dynamic seasonal storage in the following wet season—incremental growth was the most influential predictor of fall dynamic storage on both NF and SF. In our NF model, this was reflected as prior year radial increment growth, drought conditions (24–36 months), and on SF, prior summer precipitation in excess of PET contributing to variability in dynamic storage. Higher growth and transpiration linked to warmer temperatures (Carroll et al., 2014; Dagley et al., 2022) appears to result in larger end-of-season soil moisture deficits, and hence more precipitation is needed to replenish this deficit. Vegetation data did not extend through the full 60-year record, so further analysis would be needed to better evaluate D2021 in terms of radial growth and stand metrics.

Additionally, model results using data subset by years with and without logging impact aid in disentangling the effects of climate versus management. Stand density index, basal area, and harvest impact figured prominently in the predictive power of the NF post-logging model (Table 9), indicative of the effects of partial clear-cutting and pre-commercial thinning on reducing storage deficits replenished by fall precipitation. The offsite radial growth index was the only stand metric proven to be a significant predictor of storage deficits on SF for post-logging years (Table 9). This unexpected result may be due to limited and infrequent inventories of stand conditions in the Caspar watersheds and the unavailability of data for SF post-logging years after 2020. For the subset of data exclusive to harvest-impacted years, we find that offsite growth index (Navarro Redwoods, standard) best predicted the subsequent fall deficit on SF and was influential in the NF model as well. Where direct measurement of plant water use is not available, radial growth data (e.g., Carroll & Sillett, 2023) may serve as a suitable surrogate for evapotranspiration measurements.

Interestingly, in predicting precipitation antecedent to the first Q_{10} of the season, our regression models included different variables than our storage deficit models. Prior summer low flow was a significant predictor for both NF and SF, integrating the combined influence of groundwater levels, prior year(s) rainfall, and evapotranspiration. This result reflects the coupling of groundwater storage to the stream. The ratio of rainy days to total days leading up to the initial Q_{10} of the season reflects the timing and distribution of precipitation key to wetting the subsurface profile sufficiently to activate preferential flow pathways that efficiently route to the drainage network. A lengthy wet-up period with smaller, episodic rain events will not trigger the Q_{10} as efficiently as a shorter period of higher-intensity rain events where there is potentially more direct coupling of precipitation inputs to streamflow via subsurface preferential flowpaths even without complete saturation of the subsurface profile. The former case is characteristic of drought years, where we observe a delayed arrival of the first Q_{10} by approximately 2 months—a doubling of the antecedent period typical of normal or wet years (Figure 7).

4.5 | Climate trends

Regional climate station data over the period of the Caspar Creek record show significant increases in early fall and midwinter air temperatures and decreases in fall precipitation (Luković et al., 2021; Madej, 2011). In this study, spring and summer mean air temperatures increased and fall precipitation (September–November) showed a pronounced and significant decline. Declines in summer low flows have been documented in many coastal watersheds in northern California and southern Oregon (Asarian & Walker, 2016; Coble et al., 2020; Madej, 2011). In addition, Johnstone and Dawson (2010) suggest coastal summer fog frequencies have decreased since the early 20th Century, and summer fog is essential to growth dynamics in coast redwood forests (Carroll et al., 2014; Dagley et al., 2022; Sillett et al., 2022). These results highlight the importance of accounting for climatic variation in assessing the results from long-term paired watershed studies. While our results show negative trends in annual precipitation and runoff over the period of record, this trend was only significant for SF runoff. The SF trend is largely a reflection of recovery from the logging that occurred during the first decade of the streamflow record. Sillett et al. (2022) report a coast redwood growth surge from 1970 to 2000 that was linked to water availability and warming climate, concluding that more recent rising temperatures and hotter drought are diminishing coast redwood forest resilience. It remains to be seen what future perturbations to climate will do to streamflow, either directly via precipitation or indirectly changes to forest dynamics.

Consistent with findings in central Oregon by Burt et al (2014), we show that drought is a more dominant influence on streamflow than forest management. In this 60-year record, the 5 years with the lowest precipitation (1977, 2021, 2020, 2014, and 1991) include the 4 years with the lowest runoff (1977, 2021, 2014, and 1991), despite variations in stand age, basal area, and harvest-related disturbance. The year 2020 was an exception where the SF had increases in streamflow following the experimental harvest completed in 2019. With lower precipitation for the latter half of the record relative to the first, negative flow and precipitation anomalies have continued to accrue (Figure 3b).

Notably, severe streamflow drought developed in response to moderate, multiyear precipitation deficits in the early 1990s and 2009 in the absence of severe meteorologic drought. Both NF and SF experienced prolonged hydrologic drought from 1991 to 1992, resulting from a 6-year period of below-normal rainfall. The cumulative effect of this trend was 25 and 27 months of hydrologic drought on NF and SF, respectively ($SRI_{36} < -1$). SF met the definition of severe drought with intensity < −1.5 at both the 24- and 36-month integrations, while NF intensity was slightly greater than −1.5. During this 2-year period, meteorological drought was intermittent, with a maximum duration of 13 months where SPI_{36} was less than −1. Hydrologically, the 1991–1992 drought was comparable to the D2014 drought in intensity and duration, suggesting that even mild multiyear precipitation deficits may propagate to amplified hydrologic extremes. In 2009, the SF experienced a severe drought of 12-month duration and intensity of −1.7, while NF and meteorological drought intensities were −1.4 for the same duration.

4.6 | Implications for salmonids

Over the 60-year record, a significant decline in fall precipitation has delayed the onset of early-season flows needed for successful salmonid spawning migration. This result is consistent with the delayed arrival of California's rainy season (Luković et al., 2021). The delayed onset combined with low rainfall during dry years may be even more detrimental to salmonid populations in coastal streams. In addition, overall rainfall deficits accumulating since 1984 have hindered drought recovery with less surplus precipitation potentially reducing groundwater recharge, and consequently, summer baseflow and instream habitat. The lowest minimum flows of record occurred during the drought 2020. Observed stream discontinuities in what are typically perennial streams likely limited the movement of fish to avoid predation and find food during the summer of 2020.

5 | CONCLUSIONS

Our analysis of the 60-year record of precipitation and streamflow at Caspar Creek shows that harvest treatments and climatic variations interact to influence hydrologic response to meteorological drought. Increasingly lengthy, multiyear episodes of severe drought began in 1976, 2013, and 2020. By most measures, the three droughts were sequentially more severe hydrologically, reflecting longer drought durations and drier climate conditions of the 21st Century. Although the onset of hydrological drought occurred within a few months of the meteorological drought, drought persistence varied from 0 to 84 months. Hydrologic recovery from drought was more rapid after high-intensity logging in one catchment after the first drought but has yet to occur after the two 21st century droughts. Four decades after the high-intensity logging in the South Fork, drought response in that catchment was more severe than that of the North Fork, which was less intensively logged 20 years later. We attribute this drought response to enhanced evapotranspiration related to forest regrowth.

Our examination of climate trends affecting fall precipitation and streamflow thresholds revealed increasing delays in the arrival of streamflow levels adequate for successful coho salmon fall spawning migrations in small coastal streams similar to Caspar Creek. In addition to the long-term trend in these flows, adequate fall streamflow levels for salmonid migration were even more delayed during dry years as compared to normal or wet years.

Resolution of the most recent drought has yet to be observed as of September 2023. Our results suggest this recovery will depend on a multiyear pattern of surplus precipitation that percolates through the subsurface critical zone to replenish groundwater. While precipitation was a greater control on streamflow drought than forest harvesting, the interactions between multiyear weather patterns and forest harvest may have implications for long-term watershed management.

AUTHOR CONTRIBUTIONS

Elizabeth Keppeler: Conceptualization; formal analysis; methodology; visualization; writing – original draft; writing – review and editing. **Joseph Wagenbrenner:** Formal analysis; methodology; project administration; visualization; writing – review and editing. **Salli Dymond:** Project administration; visualization; writing – review and editing. **David Dralle:** Visualization; writing – review and editing.

ACKNOWLEDGMENTS

We thank the California Department of Forestry and Fire Protection (CAL FIRE) and the USDA Forest Service Pacific Southwest Research Station for funding and support of the Caspar Creek research on the Jackson Demonstration State Forest. We are grateful to Allyson Carrol for providing dendrochronology data; Jayme Seehafer, John Griffin, and Lynn Webb for assistance in compiling data; Peter Rowland for preparing maps for this report; Jim Baldwin and Nels Johnson for statistical consultation; and to our many colleagues who have collected and compiled data over the decades of research. We also thank three anonymous reviewers for their help in improving this paper.

DATA AVAILABILITY STATEMENT

The majority of the data that support the findings of this study are openly available in the USDA Forest Service Research Data Archive at https://doi.org/10.2737/RDS-2020-0017-2 and https://doi.org/10.2737/RDS-2020-0018-3. Data subsequent to 2017 are available from the corresponding author upon reasonable request.

REFERENCES

Ambrose, A.R., W.L. Baxter, C.S. Wong, R.R. Naesborg, C.B. Williams, and T.E. Dawson. 2015. "Contrasting Drought Response Strategies in California Redwoods." *Tree Physiology* 35: 453–69. https://doi.org/10.1093/treephys/tpv016.

Asarian, J.E., and J.D. Walker. 2016. "Long-Term Trends in Streamflow and Precipitation in Northwest California and Southwest Oregon, 1953–2012." *Journal of the American Water Resources Association* 52: 241–61. https://doi.org/10.1111/1752-1688.12381.

Bart, R.R., M. Safeeq, J.W. Wagenbrenner, and C.T. Hunsaker. 2021. "Do Fuel Treatments Decrease Forest Mortality or Increase Streamflow? A Case Study from the Sierra Nevada (USA)." *Ecohydrology* 14: e2254. https://doi.org/10.1002/eco.2254.

Bosch, J.M., and J.D. Hewlett. 1982. "A Review of Catchment Experiments to Determine the Effect of Vegetation Changes on Water Yield and Evapotranspiration." *Journal of Hydrology* 55: 3–23. https://doi.org/10.1016/0022-1694(82)90117-2.

Burt, T.P., N.J. Howden, J.J. McDonnell, J.A. Jones, and G.R. Hancock. 2014. "Seeing the Climate through the Trees: Observing Climate and Forestry Impacts on Streamflow Using a 60-Year Record." *Hydrological Processes* 29: 473–80. https://doi.org/10.1002/hyp.10406.

California Department of Fish and Game. 2004. "Recovery Strategy for California Coho Salmon." Report to the California Fish and Game Commission, 594 pp.

Carroll, A.L., and S.C. Sillett. 2023. "Overcoming Crossdating Challenges to Generate Ring-Width Chronologies for Sequoia Sempervirens across its Native Range." *Dendrochronologia* 78: 126063. https://doi.org/10.1016/j.dendro.2023.126063.

Carroll, A.L., S.C. Sillett, and R.D. Kramer. 2014. "Millennium-Scale Crossdating and Inter-Annual Climate Sensitivities of Standing California Redwoods." *PLoS One* 9(7): e102545. https://doi.org/10.1371/journal.pone.0102545.

Coble, A.A., H. Barnard, E. Du, S. Johnson, J. Jones, E. Keppeler, H. Kwon, et al. 2020. "Long-Term Hydrological Response to Forest Harvest during Seasonal Low Flow: Potential Implications for Current Forest Practices." *Science of the Total Environment* 730: 138926. https://doi.org/10.1016/j.scitotenv.2020.138926.

Costanza, J.K., F.H. Koch, and M.C. Reeves. 2023. "Future Exposure of Forest Ecosystems to Multi Year Drought in the United States." *Ecosphere* 14: e4525. https://doi.org/10.1002/ecs2.4525.

Dagley, C.M., J.P. Berrill, and S. Fraver. 2022. "Forest Restoration Mitigates Drought Vulnerability of Coast Douglas-Fir in a Mediterranean Climate." *Canadian Journal of Forest Research* 53(3): 210–16. https://doi.org/10.1139/cjfr-2022-0119.

Deitch, M.J., M.V. Docto, M. Obedzinski, S.P. Nossaman, and A. Bartshire. 2018. "Impact of Multi-Annual Drought on Streamflow and Habitat in Coastal California Salmonid Streams." *Hydrological Sciences Journal* 63(8): 1219–35. https://doi.org/10.1080/02626667.2018.1492722.

Diffenbaugh, N.S., D.L. Swain, and D. Touma. 2015. "Anthropogenic Warming Has Increased Drought Risk in California." *Proceedings of the National Academy of Sciences* 112: 3931–36. https://doi.org/10.1073/pnas.1422385112.

Dralle, D.N., W.J. Hahm, D.M. Rempe, N.J. Karst, S.E. Thompson, and W.E. Dietrich. 2018. "Quantification of the Seasonal Hillslope Water Storage that Does Not Drive Streamflow: Catchment Storage that Does Not Drive Streamflow." *Hydrological Processes* 32: 1978–92. https://doi.org/10.1002/hyp.11627.

Dymond, S.F., P.W. Richardson, L.A. Webb, E.T. Keppeler, I. Arismendi, K.D. Bladon, P.H. Cafferata, et al. 2021. "A Field-Based Experiment on the Influence of Stand Density Reduction on Watershed Processes at the Caspar Creek Experimental Watersheds in Northern California." *Frontiers in Forests and Global Change* 4: 691732. https://doi.org/10.3389/ffgc.2021.691732.

Dymond, S.F., J.W. Wagenbrenner, E.T. Keppeler, and K.D. Bladon. 2021. "Dynamic Hillslope Soil Moisture in a Mediterranean Montane Watershed." *Water Resources Research* 57: e2020WR029170. https://doi.org/10.1029/2020WR029170.

Ford, C.R., S.H. Laseter, W.T. Swank, and J.M. Vose. 2011. "Can Forest Management be Used to Sustain Water-Based Ecosystem Services in the Face of Climate Change?" *Ecological Applications* 21: 2049–67. https://doi.org/10.1890/10-2246.1.

Francis, E., G.P. Asner, K.J. Mach, and C.B. Field. 2020. "Landscape Scale Variation in the Hydrological Niche of California Coast Redwood." *Ecography* 43: 1305–15. https://doi.org/10.1111/ecog.05080.

Grantham, T.E., A.L. Merenlender, and V.H. Resh. 2010. "Climatic Influences and Anthropogenic Stressors: An Integrated Framework for Streamflow Management in Mediterranean-Climate California, U.S.A." *Freshwater Biology* 55: 188–204. https://doi.org/10.1111/j.1365-2427.2009.02379.x.

Gronsdahl, S., R.D. Moore, J. Rosenfeld, R. McCleary, and R. Winkler. 2019. "Effects of Forestry on Summertime Low Flows and Physical Fish Habitat in Snowmelt-Dominant Headwater Catchments of the Pacific Northwest." *Hydrological Processes* 33(25): 3152–68. https://doi.org/10.1002/hyp.13580.

Hahm, W.J., D.N. Dralle, D.M. Rempe, A.B. Bryk, S.E. Thompson, T.E. Dawson, and W.E. Dietrich. 2019. "Low Subsurface Water Storage Capacity Relative to Annual Rainfall Decouples Mediterranean Plant Productivity and Water Use from Rainfall Variability." *Geophysical Research Letters* 46: 6544–53. https://doi.org/10.1029/2019gl083294.

Hahm, W.J., D.N. Dralle, M. Sanders, A.B. Bryk, K.E. Fauria, and M.H. Huang. 2022. "Bedrock Vadose Zone Storage Dynamics under Extreme Drought: Consequences for Plant Water Availability, Recharge, and Runoff." *Water Resources Research* 58(4): e2021WR031781. https://doi.org/10.1029/2021wr031781.

Hahm, W.J., D.M. Rempe, D.N. Dralle, T.E. Dawson, S.M. Lovill, and A.B. Bryk. 2019. "Lithologically Controlled Subsurface Critical Zone Thickness and Water Storage Capacity Determine Regional Plant Community Composition." *Water Resources Research* 55: 3028–55. https://doi.org/10.1029/2018wr023760.

Heim, R.R. 2002. "A Review of Twentieth-Century Drought Indices Used in the United States." *Bulletin of the American Meteorological Society* 83: 1149–65. https://doi.org/10.1175/1520-0477-83.8.1149.

Hermann, R.K., and D.P. Lavender. 1990. "Douglas-Fir." In *Silvics of North America: 1. Conifers. Agriculture Handbook 654*, Vol 2, edited by R.M. Burns and B.H. Honkala, 527–40. Washington, DC: U.S. Department of Agriculture, Forest Service.

Johnstone, J.A., and T.E. Dawson. 2010. "Climatic Context and Ecological Implications of Summer Fog Decline in the Coast Redwood Region." *Proceedings of the National Academy of Sciences of the United States of America* 107(10): 4533–38. https://doi.org/10.1073/pnas.0915062107.

Jones, J.A. 2000. "Hydrologic Processes and Peak Discharge Response to Forest Removal, Regrowth, and Roads in 10 Small Experimental Basins, Western Cascades, Oregon." *Water Resources Research* 36: 2621–42.

Jones, J.A., and G.E. Grant. 1996. "Peak Flow Responses to Clear-Cutting and Roads in Small and Large Basins, Western Cascades, Oregon." *Water Resources Research* 32(4): 959–74.

Keeley, J.E., and A.D. Syphard. 2021. "Large California Wildfires: 2020 Fires in Historical Context." *Fire Ecology* 17: 22. https://doi.org/10.1186/s42408-021-00110-7.

Keppeler, E.T. 1998. "The Summer Flow and Water Yield Response to Timber Harvest." In *Proceedings of the Conference on Coastal Watersheds: The Caspar Creek Story, May 6, 1998; Ukiah, CA*, edited by R.R. Ziemer, 35–43. Albany, CA: USDA Forest Service. https://doi.org/10.2737/PSW-GTR-168.

Keppeler, E.T. 2007. "Effects of Timber Harvest on Fog Drip and Streamflow, Caspar Creek Experimental Watersheds, Mendocino County, California." In *Proceedings of the Redwood Region Forest Science Symposium: What Does the Future Hold?* edited by R.B. Standiford, G.A. Giusti, Y. Valachovic, W.J. Zielinski, and M.J. Furniss, 85–94. Albany, CA: USDA Forest Service. https://doi.org/10.2737/PSW-GTR-194.

Keppeler, E.T. 2016. "Hydrologic Change in a Coast Redwood Forest, Caspar Creek Experimental Watersheds: Implications for Salmonid Survival." In *Headwaters to Estuaries: Advances in Watershed Science and Management—Proceedings of the Fifth Interagency Conference on Research in the Watersheds*, edited by C.E. Stringer, K.W. Krauss, and J.S. Latimer, 140–47. Asheville, NC: USDA Forest Service. https://doi.org/10.2737/SRS-GTR-211.

Keppeler, E.T., and D. Brown. 1998. "Subsurface Drainage Processes and Management Impacts." In *Proceedings of the Conference on Coastal Watersheds: The Caspar Creek Story, May 6, 1998; Ukiah, CA*, edited by R.R. Ziemer, 25–34. Albany, CA: USDA Forest Service. https://doi.org/10.2737/PSW-GTR-168.

Keppeler, E.T., L. Reid, and T. Lisle. 2009. "Long-Term Patterns of Hydrologic Response after Logging in a Coastal Redwood Forest." In *Proceedings of the Third Interagency Conference on Research in the Watersheds, Planning for an Uncertain Future Monitoring, Integration, and Adaptation*, edited by R.M.T. Webb and D.J. Semmens, 265–72. Denver, CO: U.S. Geological Survey Scientific Investigations Report 2009-5049. https://pubs.usgs.gov/sir/2009/5049/.

King, J.G., and L.C. Tennyson. 1984. "Alteration of Streamflow Characteristics Following Road Construction in North Central Idaho." *Water Resources Research* 20(8): 1159–63.

Lamarche, J.L., and D.P. Lettenmaier. 2001. "Effects of Forest Roads on Flood Flows in the Deschutes River, Washington." *Earth Surface Processes and Landforms* 26: 115–34.

Lenth, R.V., B. Bolker, P. Buerkner, I. Giné-Vázquez, M. Herve, M. Jung, J. Love, F. Miguez, H. Riebl, and H. Singmann. 2023. "Estimated Marginal Means, aka Least-Squares Means." 'emmeans' Package for the R Environment Version 1.9.0. https://cran.r-project.org/web/packages/emmeans/emmeans.pdf.

Lewis, J. 1998. "Evaluating the Impacts of Logging Activities on Erosion and Suspended Sediment Transport in the Caspar Creek Watersheds." In *Proceedings of the Conference on Coastal Watersheds: The Caspar Creek Story, May 6, 1998; Ukiah, CA*, edited by R.R. Ziemer, 55-69. Albany, CA: USDA Forest Service. https://doi.org/10.2737/PSW-GTR-168.

Lewis, J., S.R. Mori, E.T. Keppeler, and R.R. Ziemer. 2001. "Impacts of Logging on Storm Peak Flows, Flow Volumes and Suspended Sediment Loads in Caspar Creek, California." In *Land Use and Watersheds: Human Influence on Hydrology and Geomorphology in Urban and Forest Areas. Water Science and Application Volume 2*, edited by M.S. Wigmosta and S.J. Burges, 85–125. Washington, DC: American Geophysical Union. https://www.osti.gov/biblio/15010148.

Luković, J., J.C.H. Chiang, D. Blagojević, and A. Sekulić. 2021. "A Later Onset of the Rainy Season in California." *Geophysical Research Letters* 48: e2020GL090350. https://doi.org/10.1029/2020GL090350.

Lumley, T. 2022. "Regression Subset Selection." Leaps' Package for R Environment Version 3.1. https://cran.r-project.org/web/packages/leaps/leaps.pdf.

Madej, M.A. 2011. "Analysis of Trends in Climate, Streamflow, and Stream Temperature in North Coastal California." In *Observing, Studying, and Managing for Change—Proceedings of the Fourth Interagency Conference on Research in the Watersheds*, edited by C.N. Medley, G. Patterson, and M.J. Parker, 40–45. Fairbanks, AK: US Geological Survey Scientific Investigations Report 2011–5169. https://pubs.usgs.gov/sir/2011/5169/.

May, C.L., and D.C. Lee. 2011. "The Relationships among in-Channel Sediment Storage, Pool Depth, and Summer Survival of Juvenile Salmonids in Oregon Coast Range Streams." *North American Journal of Fisheries Management* 24: 761–74. https://doi.org/10.1577/M03-073.1.

McDowell, N.G., C.D. Allen, K. Anderson-Teixeira, B.H. Aukema, B. Bond-Lamberty, L. Chini, and J.S. Clark. 2020. "Pervasive Shifts in Forest Dynamics in a Changing World." *Science* 368: eaaz9463. https://doi.org/10.1126/science.aaz9463.

McKee, T.B., N.J. Doesken, and J. Kleist. 1993. "The Relationship of Drought Frequency and Duration to Time Scale." In *Proceedings of the Eighth Conference on Applied Climatology*, edited by T.B. McKee, N.J. Doesken, and J. Kleist, 179–84. Boston, MA: American Meteorological Society.

McLaughlin, D.L., D.A. Kaplan, and M.J. Cohen. 2013. "Managing Forests for Increased Regional Water Yield in the Southeastern U.S. Coastal Plain." *Journal of the American Water Resources Association* 49(4): 953–65. https://doi.org/10.1111/jawr.12073.

McLeod, A.I. 2022. "Kendall Rank Correlation and Mann-Kendall Trend Test." 'Kendall' Package for R Environment, Version 2.2.1. https://cran.r-project.org/web/packages/Kendall/Kendall.pdf.

Mishra, A.K., A. Alnahit, and B. Campbell. 2021. "Impact of Land Uses, Drought, Flood, Wildfire, and Cascading Events on Water Quality and Microbial Communities: A Review and Analysis." *Journal of Hydrology* 596: 125707. https://doi.org/10.1016/j.jhydrol.2020.125707.

Mishra, A.K., and V.P. Singh. 2010. "A Review of Drought Concepts." *Journal of Hydrology* 391: 202–16. https://doi.org/10.1016/j.jhydrol.2010.07.012.

National Drought Mitigation Center. 2018. "SPI Generator [Software]." University of Nebraska–Lincoln. https://drought.unl.edu/Monitoring/SPI/SPIProgram.aspx.

Neary, D.G. 2016. "Long-Term Forest Paired Catchment Studies: What Do they Tell us that Landscape-Level Monitoring Does Not?" *Forests* 7: 164. https://doi.org/10.3390/f7080164.

O'Hara, K.L., L. Narayan, and K.G. Cahill. 2015. "Twelve-Year Response of Coast Redwood to Precommercial Thinning Treatments." *Forest Science* 61: 780–98. https://doi.org/10.5849/forsci.14-178.

Perry, T.D., and J.A. Jones. 2017. "Summer Flow Deficits from Regenerating Douglas-Fir Forest in the Pacific Northwest, USA." *Ecohydrology* 10: e1790. https://doi.org/10.1002/eco.1790.

Petreshen, J. 2021. "Fog Presence and Ecosystem Responses in a Managed Coast Redwood Forest." MS thesis, University of Minnesota, Duluth, 109 pp.

PRISM Climate Group. 2020. *PRISM Climate Data*. Corvallis, OR: Oregon State University. http://prism.oregonstate.edu.

R Core Team. 2022. "R Version 4.2.2." https://www.r-project.org/.

Reid, L.M. 2012. "Comparing Hydrologic Responses to Tractor-Yarded Selection and Cable-Yarded Clearcut Logging in a Coast Redwood Forest." In *Proceedings of Coast Redwood Forests in a Changing California: A Symposium for Scientists and Managers*, edited by R.B. Standiford, T.J. Weller, D.D. Piirto, and J.D. Stuart, 151–61. Albany, CA: USDA Forest Service. https://doi.org/10.2737/PSW-GTR-238.

Reid, L.M., and J. Lewis. 2011. "Evaluating Cumulative Effects of Logging and Potential Climate Change on Dry-Season Flow in a Coast Redwood Forest." In *Observing, Studying, and Managing for Change—Proceedings of the Fourth Interagency Conference on Research in the Watersheds*, edited by C.N. Medley, G. Patterson, and M.J. Parker, 186–91. Fairbanks, AK: US Geological Survey Scientific Investigations Report 2011-5169. https://pubs.usgs.gov/sir/2011/5169/.

Restaino, C.M., D.L. Peterson, and J. Littell. 2016. "Increased Water Deficit Decreases Douglas Fir Growth throughout Western US Forests." *Proceedings of the National Academy of Sciences of the United States of America* 113(3): 9557–62. https://doi.org/10.1073/pnas.1602384113.

Richardson, P.W., P.H. Cafferata, S.F. Dymond, E.T. Keppeler, J.W. Wagenbrenner, and J.A. Whiting. 2023. "Past and Future Roles of Paired Watersheds: A North American Inventory and Anecdotes from the Caspar Creek Experimental Watersheds." *Frontiers in Forests and Global Change* 6: 1275392. https://doi.org/10.3389/ffgc.2023.1275392.

Richardson, P.W., J.E. Seehafer, E.T. Keppeler, D.G. Sutherland, and J.W. Wagenbrenner. 2021a. "Fifty-Eight Years and Counting of Watershed Science at the Caspar Creek Experimental Watersheds in Northern California." *Hydrological Processes* 35: e14207. https://doi.org/10.1002/hyp.14207.

Richardson, P.W., J.E. Seehafer, E.T. Keppeler, D.G. Sutherland, and J.W. Wagenbrenner. 2021b. *Caspar Creek Experimental Watersheds Phase 1 (1962–1985) Data*, 2nd ed. Fort Collins, CO: Forest Service Research Data Archive. https://doi.org/10.2737/RDS-2020-0017-2.

Richardson, P.W., J.E. Seehafer, E.T. Keppeler, D.G. Sutherland, J.W. Wagenbrenner, K.D. Bladon, S.F. Dymond, and R.P. Cole. 2021. *Caspar Creek Experimental Watersheds Phase 2 (1985–2017) Data*, 2nd ed. Fort Collins, CO: Forest Service Research Data Archive. https://doi.org/10.2737/RDS-2020-0018-2.

Richardson, P.W., J.W. Wagenbrenner, D.G. Sutherland, and T.E. Lisle. 2020. "Measuring and Modeling Gravel Transport at Caspar Creek, CA, to Detect Changes in Sediment Supply, Storage, and Transport Efficiency." *Water Resources Research* 56: e2019WR026389. https://doi.org/10.1029/2019WR026389.

Saksa, P., M. Safeeq, and S. Dymond. 2017. "Recent Patterns in Climate, Vegetation, and Forest Water Use in California Montane Watersheds." *Forests* 8(8): 278. https://doi.org/10.3390/f8080278.

Schwarz, G. 1978. "Estimating the Dimension of a Model." *The Annals of Statistics* 6: 461–64. https://www.jstor.org/stable/2958889.

Shive, K.L., A. Wuenschel, L.J. Harlund, A. Morris, D. Meyer, and S.M. Hood. 2022. "Ancient Trees and Modern Wildfires: Declining Resilience to Wildfire in the Highly Fire-Adapted Giant Sequoia." *Forest Ecology and Management* 511: 120220. https://doi.org/10.1016/j.foreco.2022.120110.

Shukla, S., and A.W. Wood. 2008. "Use of a Standardized Runoff Index for Characterizing Hydrologic Drought." *Geophysical Research Letters* 35: L02405. https://doi.org/10.1029/2007GL032487.

Sillett, S.C., M.E. Antoine, A.L. Carroll, M.E. Graham, A.R. Chin, and R. Van Pelt. 2022. "Rangewide Climatic Sensitivities and Non-timber Values of Tall Sequoia Sempervirens Forests." *Forest Ecology and Management* 526: 120573. https://doi.org/10.1016/j.foreco.2022.120573.

Stephens, S.L., B.M. Collins, M. Brandon, C.J. Fettig, M.A. Finney, C.M. Hoffman, E.E. Knapp, M.P. North, H. Safford, and R.B. Wayman. 2018. "Drought, Tree Mortality, and Wildfire in Forests Adapted to Frequent Fire." *BioScience* 68(2): 77–88. https://doi.org/10.1093/biosci/bix146.

Swain, D.L., B. Langenbrunner, J.D. Neelin, and A. Hall. 2018. "Increasing Precipitation Volatility in Twenty-First-Century California." *Nature Climate Change* 8: 427–33. https://doi.org/10.1038/s41558-018-0140-y.

Vicente-Serrano, S., S. Beguería, J. Lorenzo-Lacruz, J. López-Moreno, J.J. Camarero, C. Azorin-Molina, J. Revuelto, E. Morán-Tejeda, and A. Sanchez-Lorenzo. 2012. "Performance of Drought Indices for Ecological, Agricultural, and Hydrological Applications." *Earth Interactions* 16(10): 1–27. https://doi.org/10.1175/2012EI000434.1.

Vicente-Serrano, S.M., S. Beguería, and J.I. López-Moreno. 2010. "A Multiscalar Drought Index Sensitive to Global Warming: The Standardized Precipitation Evapotranspiration Index." *Journal of Climate* 23: 1696–718.

Vose, J.M., C.F. Miniat, C.H. Luce, H. Asbjornsen, P.V. Caldwell, J.L. Campbell, G.E. Grant, D.J. Isaak, S.P. Loheide, II, and G. Sun. 2016. "Ecohydrological Implications of Drought for Forests in the United States." *Forest Ecology and Management* 380: 335–45. https://doi.org/10.1016/j.foreco.2016.03.025.

Williams, A.P., J.T. Abatzoglou, A. Gershunov, J. Guzman-Morales, D.A. Bishop, J.K. Balch, and D.P. Lettenmaier. 2019. "Observed Impacts of Anthropogenic Climate Change on Wildfire in California." *Earth's Future* 7: 892–910. https://doi.org/10.1029/2019EF001210.

Wood, S.N. 2011. "Fast Stable Restricted Maximum Likelihood and Marginal Likelihood Estimation of Semiparametric Generalized Linear Models." *Journal of the Royal Statistical Society (B)* 73(1): 3–36.

World Meteorological Organization. 2012. "Standardized Precipitation Index User Guide." M. Svoboda, M. Hayes, and D. Wood. WMO-No. 1090. Geneva. 24 pp. https://public.wmo.int/en/resources/library/standardized-precipitation-index-user-guide.

Yevjevich, V. 1967. *An Objective Approach to Definitions and Investigations of Continental Hydrologic Drought. Hydrology Paper No. 23*. Fort Collins, CO: Colorado State University.

Zhang, F., J.A. Biederman, M.P. Dannenberg, D. Yan, S.C. Reed, and W.K. Smith. 2021. "Five Decades of Observed Daily Precipitation Reveal longer and more Variable Drought Events across Much of the Western United States." *Geophysical Research Letters* 48: e2020GL092293. https://doi.org/10.1029/2020GL092293.

Ziemer, R.R., and J.S. Albright. 1987. "Subsurface Pipeflow Dynamics of North-Coastal California Swale Systems." In *Erosion and Sedimentation in the Pacific Rim, Proceedings of the Corvallis Symposium*, edited by R. Beschta, T. Blinn, G.E. Grant, F.J. Swanson, and G.G. Ice, 71–80. Wallingford: International Association of Hydrological Sciences Publication No. 165.

SUPPORTING INFORMATION

Additional supporting information can be found online in the Supporting Information section at the end of this article.

How to cite this article: Keppeler, Elizabeth, Joseph Wagenbrenner, Salli Dymond and David Dralle. 2024. "Streamflow Response to Drought in a Managed Coast Redwood Catchment." *JAWRA Journal of the American Water Resources Association* 60 (5): 928–952. https://doi.org/10.1111/1752-1688.13211.